ISSN 0747-9239, Seismic Instruments, 2022, Vol. 58, No. 3, pp. 330–349. © Allerton Press, Inc., 2022.
Russian Text © The Author(s), 2021, published in Voprosy Inzhenernoi Seismologii, 2021, Vol. 48, No. 4, pp. 149–172.

Deformations, Stresses, and Strong Earthquakes in the Earth's Crust of Iran

A. A. Lukk[a], * and V. G. Leonova[a]

[a] *Schmidt Institute of Physics of the Earth, Russian Academy of Sciences, Moscow, 123242 Russia*

**e-mail: lukk@ifz.ru*

Received November 30, 2021; revised December 13, 2021; accepted December 14, 2021

Abstract—The article presents a brief overview of the currently existing ideas about the seismotectonic situation in the Earth's crust of Iran, which is experiencing intense compression in the northeastern direction as a result of collision of the Arabian and Eurasian lithospheric plates. The survey also involved geodetic data in the form of modern GPS measurements of horizontal surface displacements. The stress-strain state of the Earth's crust of Iran (construction of the average focal mechanism) was assessed based on data on the total set of 945 focal mechanisms of earthquakes of average strength ($4.4 \le M_W \le 6.5$) according to the ISC catalog, which occurred from 1975 to 2020, within 12 spatial samplings. The focal mechanisms of the strongest earthquakes in the last 50 years ($M_W = 6.0–7.4$) for one event in each of these samplings are also considered. The calculated parameters of the average mechanisms and focal mechanisms of strong earthquakes are compared both with each other and with the surrounding tectonic situation and the distribution of deformation velocity vectors according to GPS observations. A satisfactory correspondence has been established between all the comparable values. The differences in the type of formation of the seismogenic layer of the Earth's crust of Iran in different regions are demonstrated. These differences are manifested in different ratios of shear and thrust components in the reconstructed mean mechanism in different spatial samplings. A similar difference is noted in individual focal mechanisms of the strongest earthquakes. However, it is possible to describe the observed nature of deformation of the crust of Iran within a single concept of collisional tectonics, caused by collision of the Arabian and Eurasian plates in the last 5 Ma.

Keywords: collisional tectonics, fold–thrust belt, stress-strain state, medium mechanism, strong earthquake focal mechanism, compression, thrust, strike-slip

DOI: 10.3103/S0747923922030100

INTRODUCTION

Iran with its immediate environment is one of the most seismic intracontinental areas of the world. It is extremely important to understand exactly what is responsible for the occurrence of strong destructive earthquakes in this area.

The vast majority of modern publications on the seismicity, tectonics, and nature of Iran's deformation present the corresponding material from the standpoint of plate tectonics, which has defined our presentation of the corresponding materials in this article.

One of the most reliable postulates of plate tectonics is recognition of detachment of the Arabian from the African Plate along the Red Sea about 200–300 Ma ago and its independent movement at a rate of about 3 cm/year NNE towards motionless Eurasia, the southern margin of which is precisely represented by the Iranian microplate (Vernant et al., 2004a).

The territory of present-day Iran, located on this passive microplate in the past, during the Mesozoic–Cenozoic was subjected to continental collision between the mobile Arabian and immobile Eurasian plates. Their collision began 35 Ma ago, when the peripheral margin of the Arabian Plate, which had negative buoyancy, was pushed under the upper Iranian microplate. In connection with this subduction, thickening of the Iranian crust began ~25 Ma ago, which is confirmed by exhumed rocks of inner Iran and detrital deposits of the Mesopotamian foredeep, the foreland of the Arabian Plate (Mouthereau et al., 2012). However, the main uplift, deformation, and exhumation throughout the entire Arabia–Eurasia collision zone began later, ~12–15 Ma ago. It was then that the Zagros Mountains were born as a result of progressive shortening/thickening of the initially weak crust of Iran, accompanied by the hypothetical subduction of the stronger, brittle crust of the Arabian plate under it. It is suggested that thickening of the Iranian crust caused by this underthrust is one of the main reasons for the uplift of the Zagros region and the Iranian Plateau in general (Allen et al., 2003, 2004, 2011; Talebian and Jackson, 2004).

In southeastern Iran, north of the Omani Coast, there appears to be a sharp transition from fold–thrust orogeny in the Zagros to a subduction regime in the Makran region. Such a change in tectonic regime is indicated by numerous geological and tectonic evidence of modern subduction of the bottom of the Arabian Sea under the coast of Makran (e.g., (Jackson and McKenzie, 1984; Maggi et al., 2000)).

All these issues, along with tectonics and seismicity, have been the subject of active study over the past 20–30 years, since the territory of Iran provides a rare opportunity to observe and quantify how the convergence between the two plates—the Arabian and Eurasian—took place from its beginning to its current continuation, i.e., before the continental collision of these plates in Iran. In addition, Iran is the site of frequent destructive earthquakes and is therefore extremely important for understanding how these earthquakes occur against the background of this collision.

This article is another attempt to understand the relationship between tectonic deformations, stresses, and the location of strong destructive earthquakes in the crust of Iran. At the same time, we have extensively used the results of numerous earlier studies in this direction, which served as the starting point for our own research.

ELEMENTS OF TECTONICS AND SEISMICITY OF IRAN

Modern tectonics determines the kinematics of the Arabian–Eurasian collision over the past 5–10 Ma. It is expressed by a series of dextral strike-slip faults on the Turkish–Iranian Plateau between 48° and 57° E. The strikes of these faults vary from NW–SE to NW–SSE. Some faults are seismically active and/or show geomorphological evidence of Holocene origin, which indicates their tectonic activity. The main ones are shown in Fig. 1.

The displacements along these faults, estimated from geological and geomorphological features based on satellite images, digital topography, geological maps and modern field observations, range from several tens to several hundreds of kilometers (Talebian and Jackson, 2002; Allen et al., 2004, 2011, 2013; Vernant et al., 2004a, 2004b; Horton et al., 2008; Walpersdorf et al., 2014; Bachmanov et al., 2019). Together, these faults are assumed to absorb a significant part of convergence of the Arabian and Eurasian plates. This strike-slip faulting of the crust of Iran implies, in turn, elongation along the strike of the collision zone, in which the Anatolian block, bounded by the dextral North Anatolian and sinistral South Anatolian faults, is pushed to the west. Thrust formation is also concentrated in the Zagros and Alborz mountains.

These deformations of the crust of Iran determine the intense seismicity of the Anatolian microplate and Zagros and Alborz mountain structures. The central part of the Iranian Plate is weakly subjected to deformations, which is confirmed by its almost complete aseismicity. This testifies in favor of the high rigidity of crustal material in this part of Iran. To some extent, a similar situation is also observed in eastern Iran within the almost aseismic rigid Lut block, which is seismic along its margins and is concentrated in pronounced subparallel fault systems of submeridional (on the eastern and western margins of the block) and sublatitudinal (on its northern and southern margins) strike.

At the eastern end of the Zagros fold–thrust belt, within Oman coast, there is apparently a sharp change in the tectonic regime from fold–thrust orogeny in the Zagros to a subduction regime in the Makran region (e.g., (Jackson and McKenzie, 1984; Maggi et al., 2000)). In contrast to the Zagros fold–thrust belt, the presence of seismicity is noted here not only in the upper horizon of the crust, but also at sufficiently large depths in the lithosphere down to 150 km (Engdahl et al., 2006). The seismogenic surface is inclined to the north under the relatively rigid Lut block and Afghan continental block of the subducting Arabian Plate (see (Engdahl et al., 2006, Figs. 9a, 10)).

As well, the Oman region is a geologic syntaxis where the longitudinal NE–SE trending Zagros faults and folds bend sharply to a submeridional strike to join the Makran Fault Zone in the south. The region is a transition from continental–continental collision at the Zagros to subduction of the Arabian Plate under the Makran Coast (Regard et al., 2004, 2005). The depth of earthquake sources in this transition zone increases northward from 8–12 km near the coast to ~30–40 and 50 km north of the Zagros geological suture between Arabian and Iranian rocks (Talebian and Jackson, 2004).

The concept of the spatial structure of seismicity and the location of strongest earthquakes in Iran with $M_W \geq 7.0$ from prehistoric time to 2018 can be obtained by considering Fig. 2 (see also (Koronovsky et al., 2017)). It also shows the division of Iran into various seismotectonic units both based on this seismological information and all available geological, geophysical, and tectonic data (Mousavi-Bafrouei and Mahani, 2020).

Six main seismotectonic provinces have been identified: (1) the Zagros continental–continental collision zone in southwestern Iran (ZG in Fig. 2); (2) highly seismic regions of Alborz and Azerbaijan with the Talesh mountain range in the extreme west (AA); (3) the intraplate weakly seismic environment of Central Iran (CN); (4) the Kopetdag continental collision zone in the northeast (KD); (5) the weakly deformable rigid Lut block (L); (6) the Makran oceanic–continental subduction zone in the southeast (MK), which is distinguished in a number of studies of the seismicity of Iran (see, e.g., (Mousavi-Bafrouei and Mahani, 2020)).

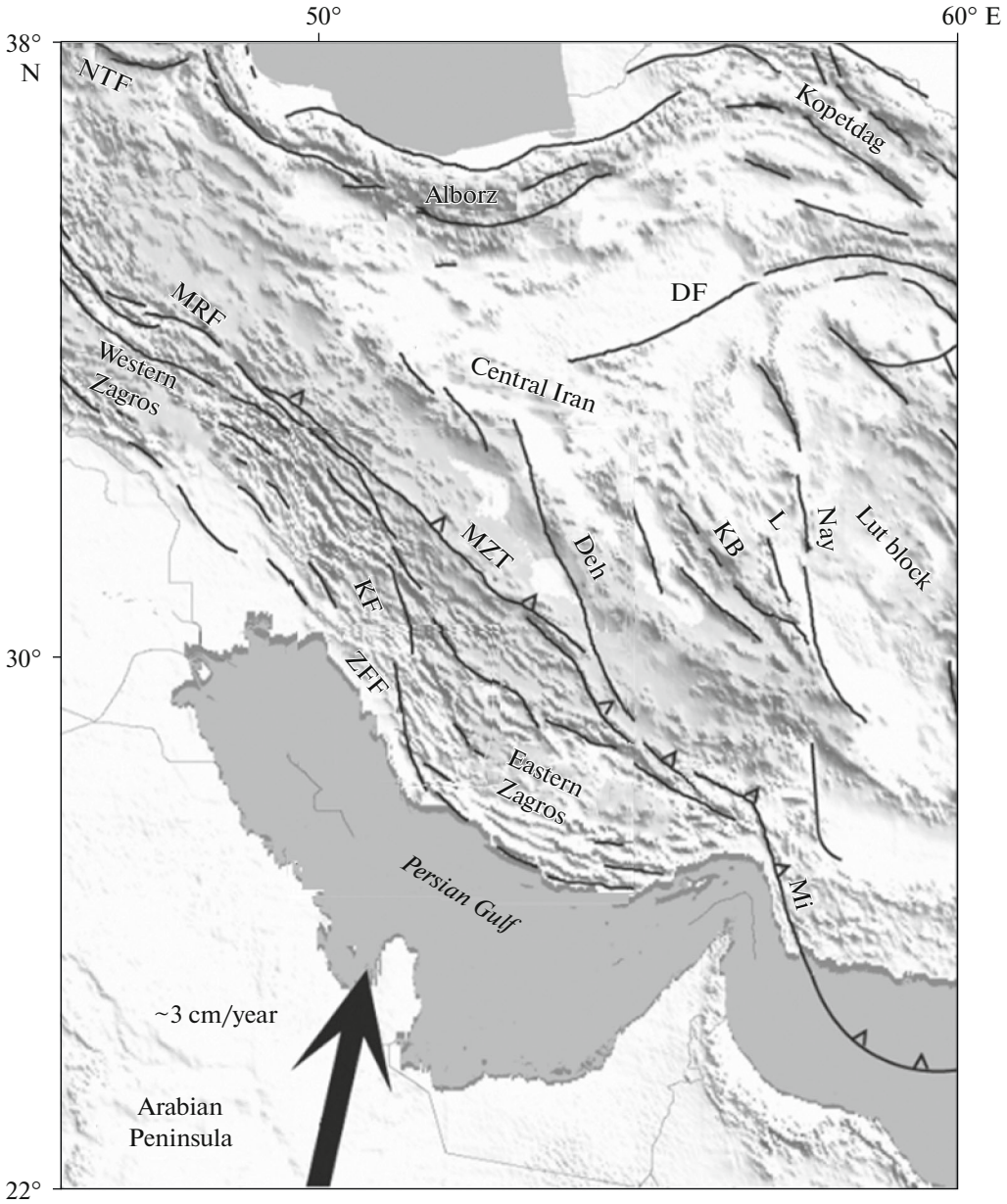

Fig. 1. Fragment of simplified tectonic map of Iran (after (Vernant et al., 2004), with changes after (Lukk and Rebetsky, 2018)). MRF, Main Recent Fault; NTF, North Tabris Fault; MZT, Main Zagros Thrust; ZFF, Zagros Frontal Fault; KF, Kazerun Fault; DF, Dorouneh Fault; Deh, Dehshir Fault; KB, Kuh Banan Fault; Nay, Nayband Fault; L, Lakarkuh Fault; Gowk, Gowk Fault; Mi, Minab Zendan Palami fault zone. Arrow shows direction of movement of Arabian Plate relative to Eurasia according to NUVEL-1A model (DeMets et al., 1994).

According to Fig. 2, seismicity is generally concentrated in the Zagros mountain belt, the Alborz–Azerbaijan–Talesh and Kopetdag segments, along the boundaries of the rigid Lut block, as well as dispersed relatively strong earthquakes in the Makran subduction zone in the extreme southeast of Iran. The central part of Iran, represented by the rigid core of the Iranian Plate, and the central part of the rigid Lut block, are virtually aseismic.

IRAN'S CRUSTAL DEFORMATION BASED ON GPS OBSERVATIONS

In this section, we summarize the present-day crustal deformations in Iran measured to date by a number of geodetic GPS observation network services in Iran from 1997 to 2013 (Tatar et al., 2002; Nilforoushan et al., 2003; Vernant et al., 2004a, 2004b; Masson et al., 2005, 2006, 2007, 2014; Bayer et al., 2006; Hessami et al., 2006; Walpersdorf et al., 2006,

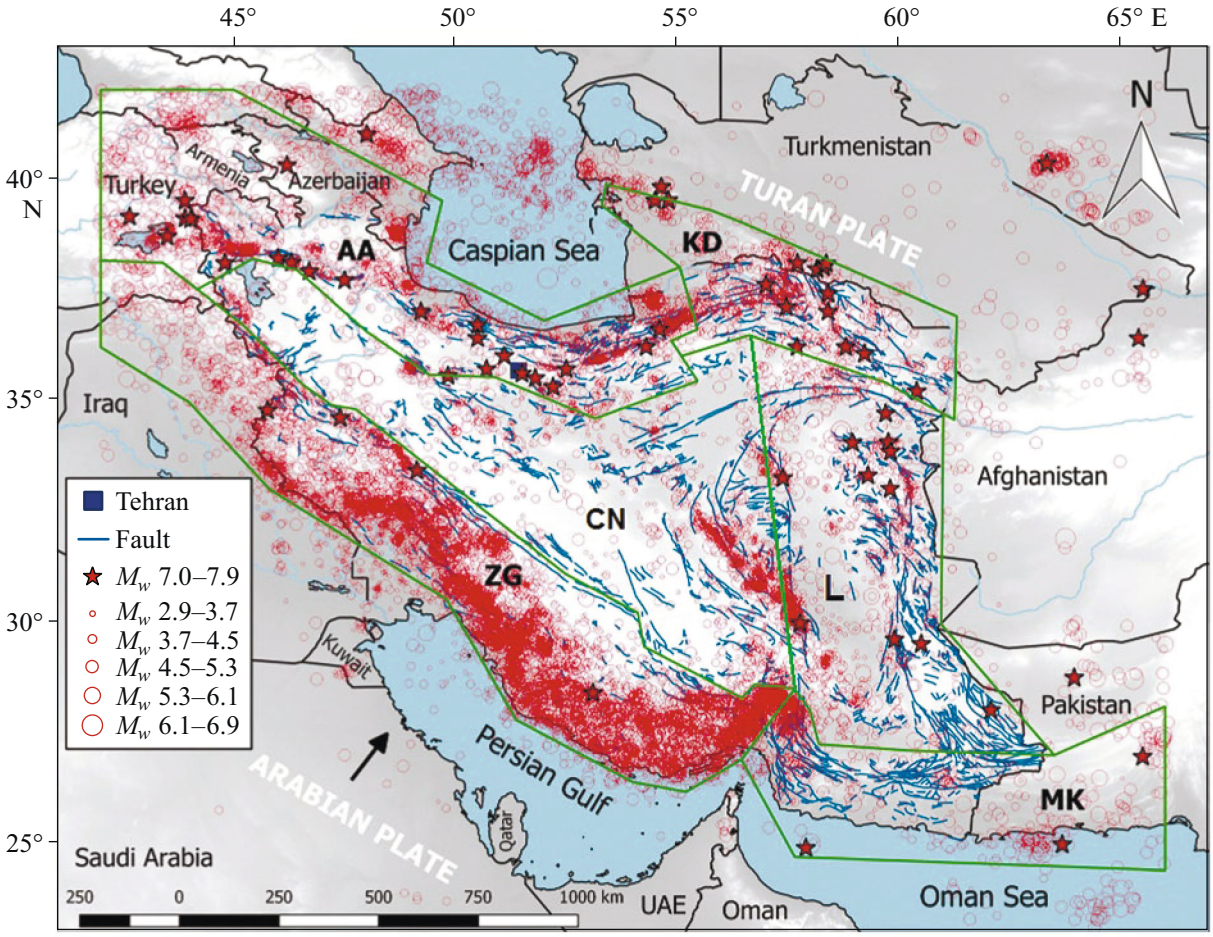

Fig. 2. Map of Iran showing seismotectonic units (AA, Alborz–Azerbaijan; CN, Central Iran; KD, Kopetdag; ZG, Zagros; L, rigid Lut block; MK, Makran collision zone) and its immediate environment. Circles, earthquake epicenters with $2.9 \le M_W \le 6.9$ from prehistory to 2018; asterisks, strong earthquakes with $M_W \ge 7.0$. Fault, tectonic faults (after (Mousavi-Bafrouei and Mahani, 2020)).

2014; Tavakoli et al., 2008; Peyret et al., 2009; Jamor et al., 2010, 2011; Mousavi et al., 2013; Raeesi et al., 2017; Khorrami et al., 2019). Khorrami et al. (2019) show the field of movement velocities for the IPGN network (Iranian Permanent GNSS Network) based on the above data collected from 2006 to the end of 2015. This solution was used as a reference velocity field against which all previously published velocity fields were equalized ((Reilinger et al., 2006; Raeesi et al., 2017)). The calculated residual horizontal velocities have RMS values of 0.89 mm/yr for 64 common points with the solution (Raeesi et al., 2017) and 0.33 mm/year for 9 common points with the solution (Reilinger et al., 2006). Khorrami et al. (2019) obtained a matched set of coordinates and velocities in the ITRF2014 system (Altamimi et al., 2016), which is shown in Fig. 3.

According to Fig. 3, the direction of convergence of the Arabian Plate with Eurasia changes from NNW in the western half of Iran to NNE in its eastern half. The rate of approach increases from ~19 mm/yr at 48° E to ~27 mm/yr at 58° E. East of 58° E, most of the shortening occurs via subduction of Makran, while the rest is absorbed by the Kopetdag range. The difference between the velocities of sites on the Makran Coast and those on the Gulf of Oman coast also suggests that the subduction rate increases from west to east. West of 58° E, the shortening is distributed between Zagros, Alborz, and the Caucasus. This difference causes shear displacement. Between Central Iran and the Helmand block, located east of the rigid Lut block, shear displacement also occurs, apparently due to an increase in the subduction rate in this direction. The rates of GPS points located east of the Iranian border are very low, and this suggests that the Helmand block is part of the Eurasian Plate (Jackson and McKenzie, 1984; Vernant et al., 2004a).

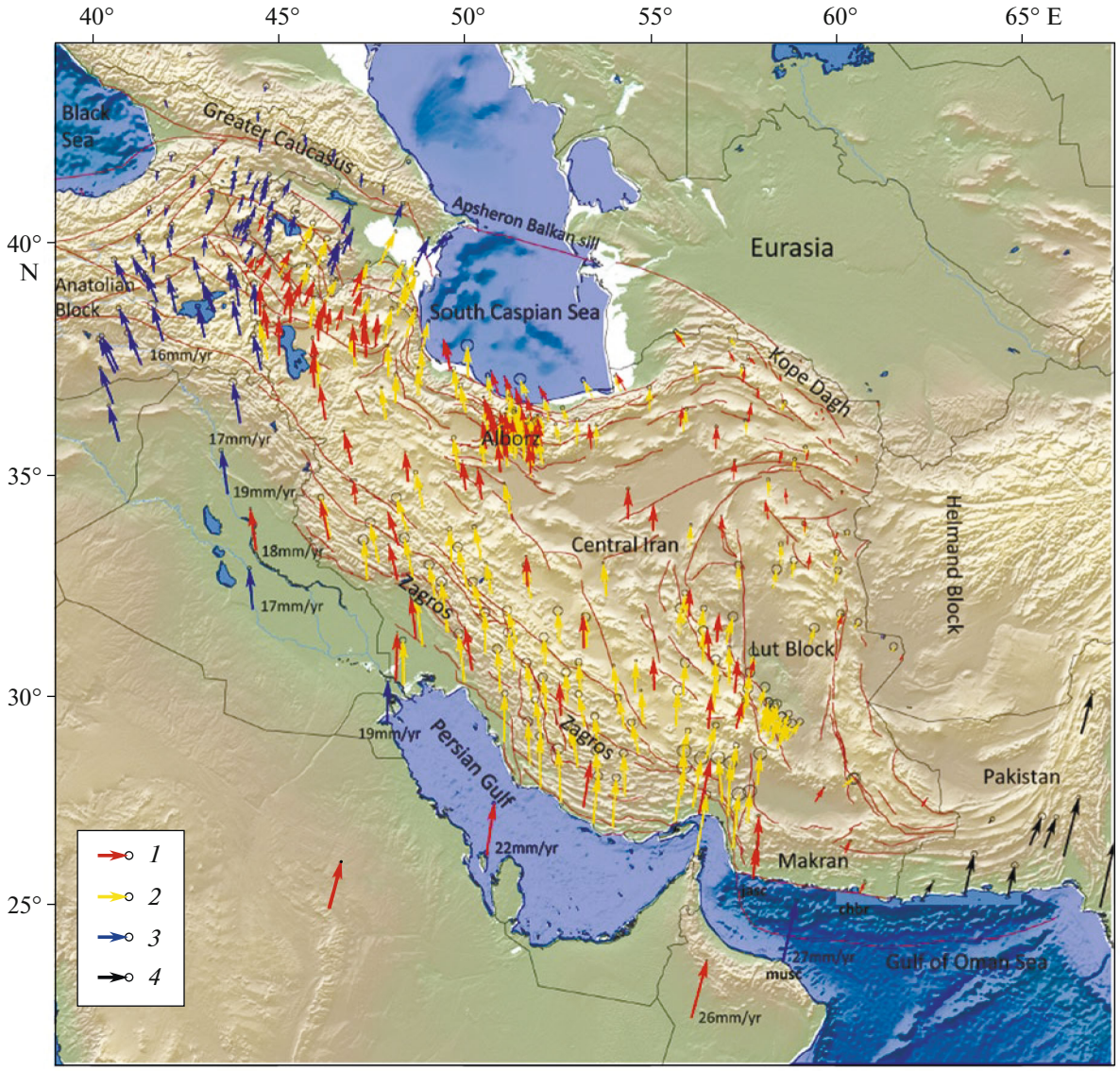

Fig. 3. Unified velocity field based on GPS observations with respect to fixed Eurasia (arrows *1*, after (Khorrami et al., 2019)); *2*, solution (Raeesi et al., 2017); *3*, solution (Reilinger et al., 2006); *4*, solution (Frohling and Szeliga, 2016). All GPS velocity fields have been converted to IPGN datum (arrows *1*).

The transpressional tectonic regime (shear compression) caused by the collision of the Arabian and Iranian plates regulates the activity of all strike-slip faults in Iran (Hessami et al., 2006). In addition, it transfers this activity west of Iran, along the Arabian Cape, where strike-slip movement along the Main Recent Fault (MRF) further northwest into the dextral strike-slip North Anatolian Fault (NAF), along which the Anatolian Plate moves into the Hellenic collision zone (Authemayou et al., 2009). At the same time , the northern part of the Iranian Plateau, the Talesh mountain range, and the Lesser Caucasus are moving to the northeast.

Figure 4 shows the distribution of the strain rate tensor derived from the velocity field shown in Fig. 3. The focal mechanisms of earthquakes from 1976 to 2016 are also shown here according to the Harvard CMT solutions (Khorrami et al., 2019). In Fig. 4, the following first-order features are observed: (1) significant shortening between Arabia and southern Iran over the Makran Trench; (2) the Oman transitional zone between the Zagros fold–thrust belt and the Makran subduction (54° E–58° E) with right-lateral movement associated with the Minab–Zendan–Palami (MZP) fault system; (3) a decrease in the rate of compression from the Eastern to Western Zagros; (4) a right-lateral fault pattern in northwestern Iran and eastern Turkey along the North Tabriz fault (NTF), the Gailatu–Siah-Ceshmeh–Khoy (GSK) fault and the Halderan fault and its continuation along

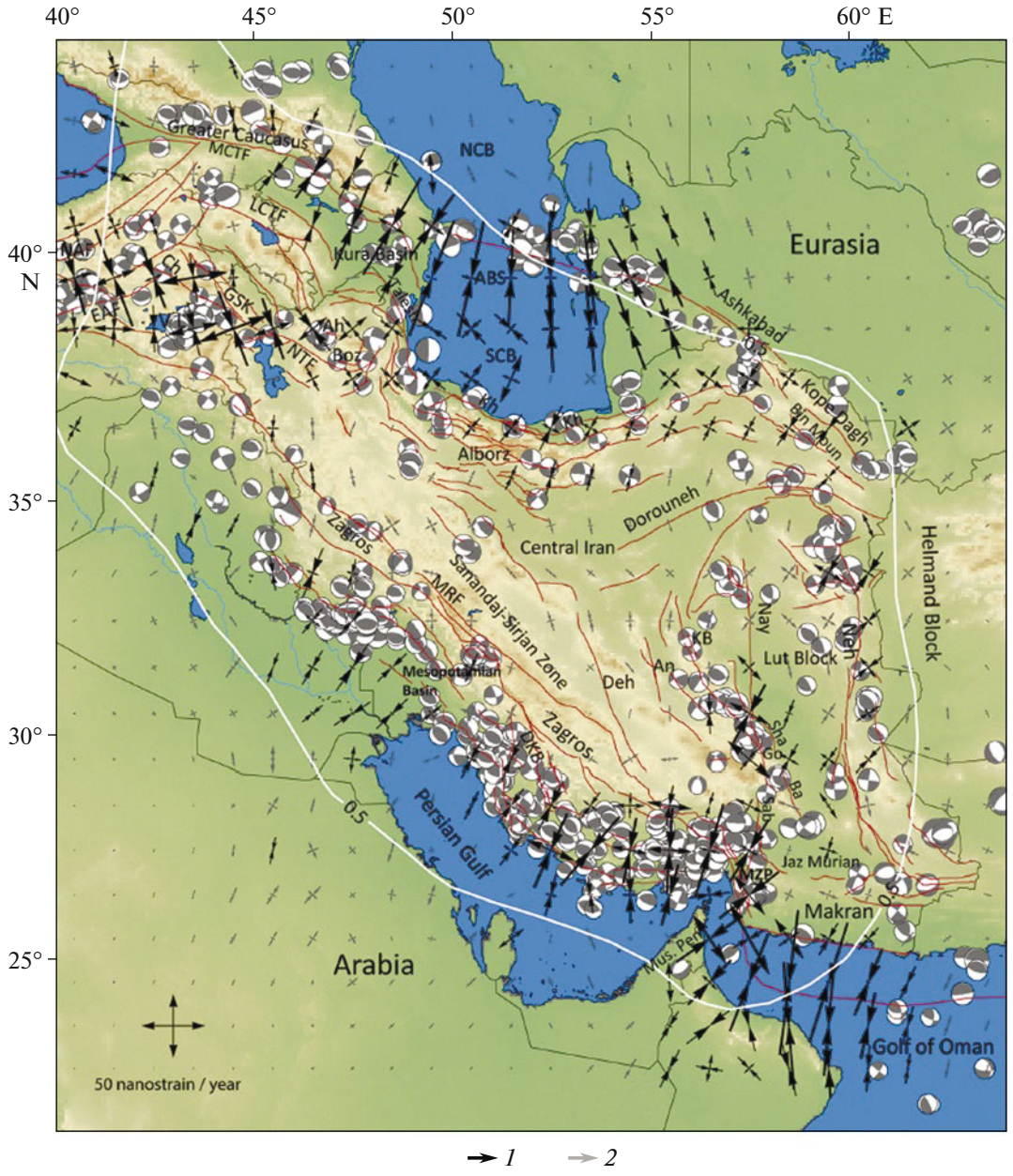

Fig. 4. Strain rate tensor calculated from velocity field in Fig. 3 to scale of Iran (grid step 1°) (after (Khorrami et al., 2019)). Black arrows, high strain rates (more than 2.0 mm/100 km per year); gray arrows, low strain rates (less than 2.0 mm/100 km per year). Focal mechanisms from 1976 to 2016 according to Harvard CMT solutions. White line, area where diagonal term of resolution matrix exceeds 0.5. ABS, Absheron–Balkan high; Ah, Ahar fault zone; An, Anar; Ba, Bam; BinMoun, Binalud Mountains; Boz, Bozgush (Mt. Bozgush); Ch, Chalderan; Deh, Dehshir; DKB, Dena–Kazerun–Borzajan; EAF, East Anatolian Fault; GSK, Gailatu–Siah Cheshmeh–Khoy Fault; Go, Gowk; KB, Kuhbanan (Kuhbanan); LCTF, Lesser Caucasus Thrust Fault; MRF, Main Recent Fault; MCTF, Main Caucasus Thrust Fault; Mus. Pen, Musandam Peninsula; MZP, Minab–Zendan–Palami fault system; NAF, North Anatolian Fault; Nay, Nayband; Neh, Nehbandan fault system; NTF, North Tabriz Fault; NCB, North Caspian basin; SCB, South Caspian basin; VL, Lake Van.

the North Anatolian fault (NAF) in Turkey; (5) significant shortening throughout the northern part of the Kura River basin and the southern part of the Greater Caucasus in Azerbaijan; (6) a pure meridional compressive regime of the Absheron–Balkhan stratum (ABS).

It also confirms the separation of the type of deformation in the Western Zagros into shortening along the southern front and dextral slip along the Main Recent Fault (MRF) in a first approximation. This fault is the boundary between the Western Zagros and the quasi-rigid area of Sanandai-Sirjan located north

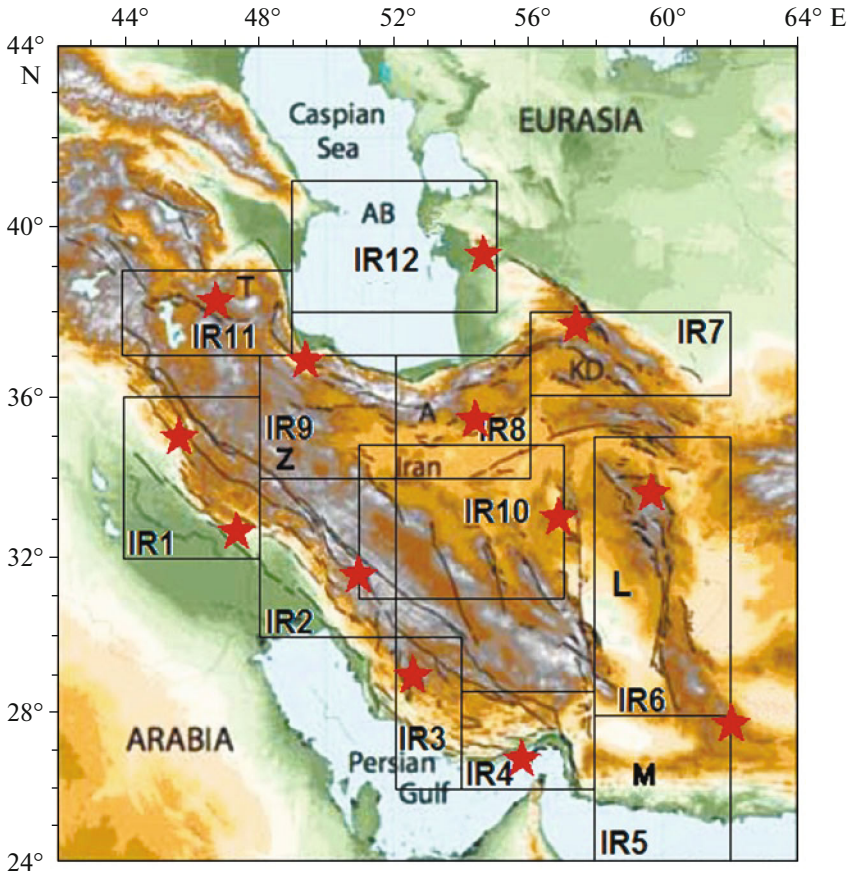

Fig. 5. Position of spatial samplings (IR1–IR12) on territory of Iran for calculating average mechanisms and epicenters of strongest earthquakes for 1970–2020 (geographical basis after (Engdahl et al., 2006)). Z, simple Zagros fold–thrust belt; M, Makran subduction zone; L, rigid Lut block; KD, Kopetdag; A, Alborz Range; Iran, Central Iranian Plateau; T, Talesh mountain range; AB, Absheron–Balkhan underwater ridge.

of it in the Central Iranian block. Movement along the MRF is transferred to the southern front of the Eastern Zagros via the Kazerun (Borodzhan) system of dextral strike-slip faults. In the Eastern Zagros, deformations are concentrated mainly on the southern front and in the transition zone between the Zagros–Makran subduction zone; this transition results from the Minab–Zendan–Palami system with a total dextral shear rate of ~17 mm/year.

CALCULATION OF THE STRESS-STRAIN STATE IN VARIOUS REGIONS OF IRAN FROM DATA ON THE FOCAL MECHANISMS OF EARTHQUAKE SOURCES

Using all of the above considerations regarding the possibility of subdividing Iran into various seismogenic structures, we compiled a series of spatial samplings within which we calculated the characteristics of the stress-strain state from sets of earthquakes with $M_W \geq 4.4$ according to the ISC catalog (International..., 2021) for 1975–2020, by constructing the average focal mechanism (Yunga, 1990). These samplings are shown in Fig. 5.

Samplings IR1–IR4 correspond to the Zagros fold–thrust belt; sampling IR5, to Makran subduction zone; IR6, to the rigid Lut block; IR7, to the Kopetdag seismogenic zone; IR8, to the eastern branch of the Alborz range; IR9, to the western branch of the Alborz range; IR10, to the central part of the Iranian Plateau; IR11, to the Talesh mountain range in the Alborz–Azerbaijan seismogenic zone; IR12, to the high of the Absheron–Balkhan underwater ridge in the Caspian Sea.

Within these samplings, the average focal mechanisms of sets of earthquakes with $M_W \geq 4.4$ according to the ISC catalog for 1975–2020 were calculated. The results are plotted in Fig. 6. The corresponding calculated parameters of the stress-strain state (SSS) estimated by these average mechanisms are given in Table 1.

According to Fig. 6 and Table 1, thrust formation predominates in the Zagros fold–thrust belt. The principal axis of compression (P) is almost horizontal

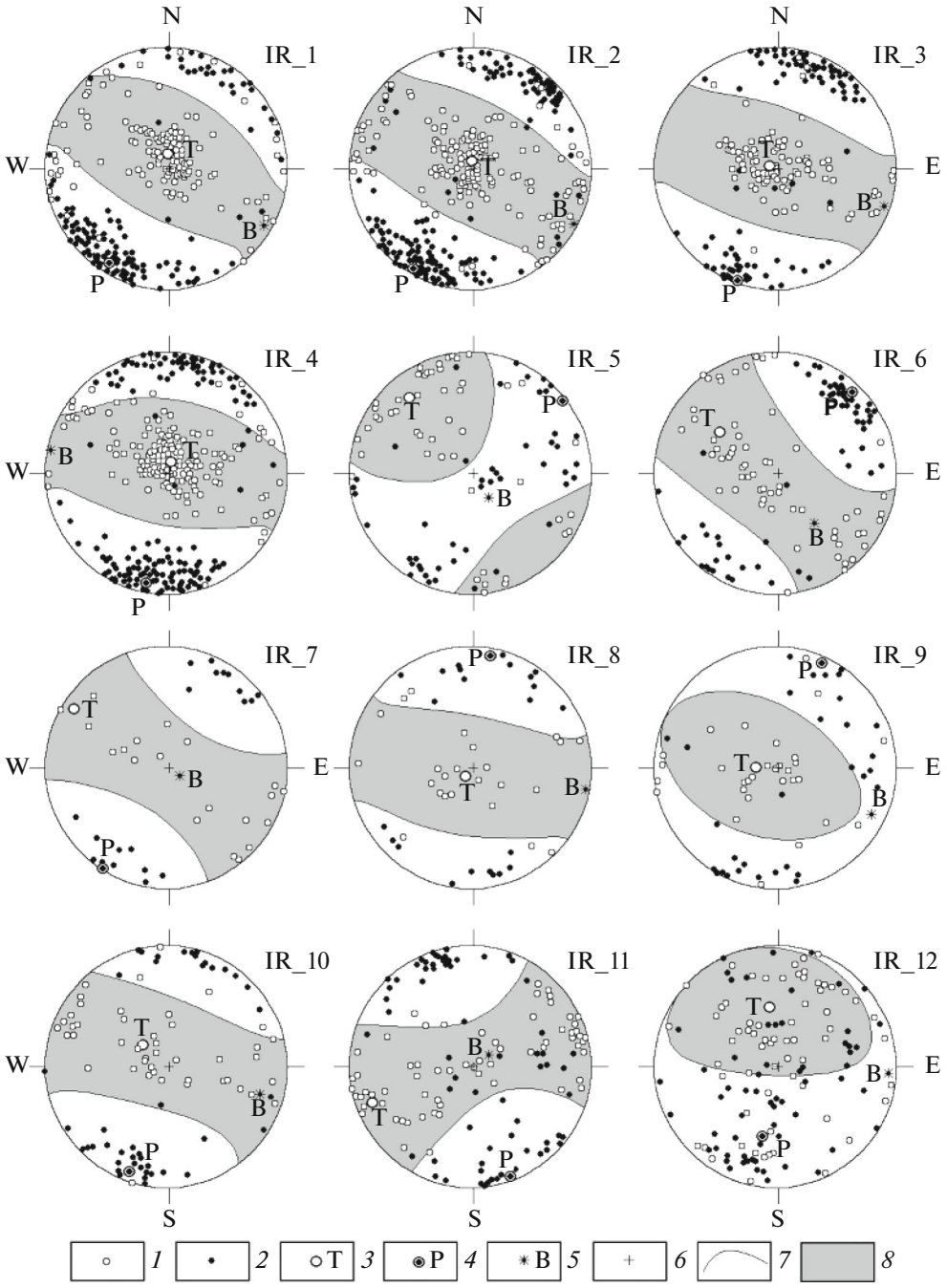

Fig. 6. Results of calculating average mechanisms for various spatial samplings on territory of Iran according to ISC catalog for 1975–2020. *1*, Exit to surface of lower hemisphere of principal axes of extension for individual focal mechanisms; *2*, same for principal axes compression of individual mechanisms; *3*, exit to surface of lower hemisphere of principal axis of extension (T) of average mechanism; *4*, same for principal axis of compression (P) of average mechanism; *5*, same for neutral axis (B); *6*, center of stereographic projection; *7*, trace on lower hemisphere of nodal planes; *8,* extension zone in average mechanism solution.

and is oriented across the strike of the belt. Clearly pronounced rotation of the compression axis from 211° to 190° is noted as it moves from the northwestern part of Zagros (IR1) to its southeastern extremity (IR4). This rotation is due to the corresponding rotation of the Zagros strike, which is distinctly visible in Figs. 1 and 2. The type of SSS, obtained as a result of calculations, corresponds to tectonic concepts about the predominant thrust formation in the Zagros range.

This thrust formation is abruptly replaced by an extension-dominated setting at an azimuth of 322° within the inferred Makran subduction zone (IR5).

Table 1. Stress-strain state parameters in various spatial samplings in Iran according to data on earthquake focal mechanisms for 1975–2020

Area	N	Main axes of average mechanism						k	μ_M	Type of SSS
		T		B		P				
		Azm	α	Azm	α	Azm	α			
IR1	139	007	80	120	04	211	10	0.65	0.187	Thrust
IR2	176	020	84	118	01	208	05	0.63	0.360	Thrust/compression
IR3	103	296	86	109	04	199	00	0.68	0.375	Thrust/compression
IR4	162	025	82	280	02	190	08	0.67	0.180	Thrust
IR5	049	322	21	143	69	052	00	0.45	–0.390	Extension/strike-slip
IR6	062	307	43	141	46	044	07	0.62	0.699	Compression
IR7	020	302	10	121	80	212	00	0.71	0.660	Compression
IR8	024	212	84	100	02	010	06	0.52	0.390	Strike-slip/compression
IR9	031	274	77	115	12	025	04	0.46	–0.067	Thrust
IR10	045	314	69	106	19	199	09	0.58	0.638	Compression
IR11	069	250	15	060	75	159	02	0.51	0.402	Strike-slip/compression
IR12	065	354	49	094	08	190	40	0.20	–0.204	Slice–Incision

N, number of focal mechanisms used; Azm, α, orientation (azimuth and inclination to horizon) of principal stress axes of average mechanisms; *k*, reliability of determining average mechanism ($0 \le k \le 1$); μ_M, Lode–Nadai coefficient ($-1 \le \mu_M \le +1$), which determines type of stress-strain state (SSS).

The sharp change in the type of SSS corresponds to the tectonic concept of a change in the thrust formation setting in Zagros to a setting of subducting oceanic crust in the Gulf of Oman under continental crust in the Makran subduction zone. In the same region, some predominance of tensile strain is noted based on geodetic measurements (see Fig. 4). Thus, our estimates of the type of SSS in southern and southeastern Iran are in accordance with ideas about the nature of deformation of this part of Iran based on the geological and geodetic data.

The Lut block (IR6), according to our calculations, is under conditions of intense compression (μ_M = 0.699) at an azimuth of 44°. According to modern tectonic concepts (see, e.g., (Allen et al., 2004; Vernant et al., 2004a; Walker and Jackson, 2004; Walpersdorf et al., 2014)), it is bounded in the west and east by well-defined active meridional strike-slip zones, along which shear displacement occurs between Central Iran and the Helmand block located to the east of the Lut block (Walpersdorf et al., 2014). The rates of GPS stations located east of the Iranian border near the western margin of the Helmand block are very low (see, e.g., Fig. 3), and this suggests that the Helmand block located east of the Lut block is part of the Eurasian Plate (Jackson and McKenzie, 1984; Vernant et al., 2004a). This information, together with our solution of the type of SSS within the Lut block—the orientation of subhorizontal compression at an azimuth of 44°, which determines the dextral shear displacement of the Lut block—makes it possible to suggest that, within it, protrusion of the Arabian plate is actively indenting northward into the crust of Eurasia.

Predominant horizontal compression observed by us (μ_M = 0.66) at an azimuth of 32° (212°) within the Kopetdag range (IR7) determines the intense thrusting in this range with a strike at an azimuth of ~120°–130°. Precisely this tectonic setting is noted in the literature for this territory (see, e.g., (Hollingsworth et al., 2006; Walker et al., 2009). For the Eastern (IR8) and Western (IR9) Alborz, there is a submeridional thrust formation setting with a significant compression component in the Eastern Alborz (μ_M = +0.4) in contrast to the almost pure thrust formation in the Western Alborz (μ_M = –0.07). In the first case, the horizontal compression is oriented in the direction of 10°, and in the second case, 25°. The certain difference in the direction of compression is most likely determined by the northward turn of the strike of the Western Alborz from the sublatitudinal strike of its eastern part (see Figs. 1 and 2). The same thrust formation setting is observed in the Alborz range based on the geological data (see, e.g., (Jackson et al., 2002; Allen et al., 2003, 2013; Masson et al., 2006)).

In the central part of the Iranian Plateau (IR10), there is a setting with predominant horizontal compression (μ_M = 0.68) in the same direction as in more southerly located cells IR2 and IR3 in the Zagros fold–thrust belt. The differences consist only in the predominant intensity of this compression in the plateau versus the Zagros fold–thrust belt (μ_M = 0.36–0.38).

For the Talesh ridge (IR11) there is shear with a lateral compression component. The orientation of the subhorizontal compression (P) and tensile (T) axes matches the strike of the fault system in the Talesh ridge in the northwestern–southeastern direction (see, e.g., Fig. 3).

For the Asheron–Balkhan underwater ridge (IR12), an incision setting is observed that is atypical of other areas along the sublatitudinally trending subvertical plane. This agrees well with the sublatitudinal strike of the step in the basement in the subaqueous part of the Caspian Sea within the limits of the underwater ridge.

Thus, it can be argued that the solutions we obtained for the SSS of the seismogenic layer of the crust in various parts of Iran agree well with the tectonic setting within them.

THE STRONGEST EARTHQUAKES IN THE LAST 50 YEARS WITHIN VARIOUS REGIONS OF IRAN

Within the above-mentioned different regions of Iran, one of the strongest earthquakes in the last 50 years was selected from the ISC catalog with determined focal mechanisms. The epicenters of these strongest events are shown in Fig. 5. Table 2 presents the time of occurrence of earthquakes (according to the NEIC catalog), the coordinates of epicenters, and magnitudes of earthquakes (according to the NEIC and GCMT catalogs), and parameters of their focal mechanisms. For each of these seismic events, two solutions are given: the focal mechanism according to the NEIC catalog and the centroid of the moment tensor (CMT) according to the GCMT catalog. Figure 7 plots the CMT solutions with the indices (IR1–IR12) of the corresponding spatial samplings; an additional solution (IR_1-2) is shown for a strong earthquake between the strongest events of samplings IR1 and IR2.

According to Table 2, the CMT solutions of focal mechanisms according to the NEIC and GCMT catalogs are mostly quite close to each other, which testifies in favor of their stable determination.

Description of the Strongest Earthquakes in Iran

Let us describe the two strongest earthquakes in Iran in the last 50 years that are listed in Table 2.

IR1. The Iran–Iraq earthquake with $M_W = 7.3–7.4$ occurred on November 12, 2017, at the western end of the Zagros fold–thrust belt, which formed as a result of collision of the Arabian and Eurasian plates. The slip as a result of this earthquake occurred within a gentle thrust on the southern limb of the Zagros fold–thrust belt. This overthrust, located at the base of the Paleozoic rock sequence, during its displacement formed a folded anticline in the crust of this region of Iran. The fault geometry allows us to state that the width of the plunging fault plane (according to its dip) is about 30 km, which is quite consistent with accumulation of tectonic stresses sufficient for the occurrence of a strong earthquake of this magnitude. In the preferred earthquake slip model, two sections are distinguished with a maximum slip of 6 m, offset by 16 km, which implies a significant change in frictional properties within the rupture plane (Feng et al., 2018). Near the epicenter of the earthquake, Mt. Bamo rose by about 1 m, which can be considered evidence of strong earthquakes in the development of thrust formation and folding of the Zagros fold–thrust mountain belt in the studied area.

It should be noted that the focal mechanism of this strong earthquake agrees with the type of the average mechanism established by us from a set of 139 focal mechanisms of medium-strength earthquakes ($4.4 \le M_W \le 6.3$) that occurred in this spatial sampling according to the ISC catalog for 1975–2020 (see Fig. 6); both of these solutions agree with existing ideas on the fold–thrust orogeny in the Zagros mountain belt. The working slip plane during a strong earthquake is spatially located with respect to the thrust fault plane identified here from the geological data, which is part of a NW–SE fault system, in the southern limb of the Zagros (a possible continuation of the Zagros frontal fault—ZFF in Fig. 1). The location of this strong earthquake and nature of seismic movement in its source fully correspond to tectonic ideas about thrusting of rocks of the Arabian high here onto the crust of Iran.

IR_1-2. A strong earthquake with $M_W = 6.2$ occurred on August 18, 2014, in the Zagros Mountains at the boundary of sites IR1 and IR2. It was accompanied by a sequence of five events with $M_W \ge 5.4$. Both the main shock and accompanying aftershock sequence were characterized by predominantly thrust mechanisms and had centroid depths corresponding to the position of a thick sedimentary sequence above the crystalline basement. This earthquake sequence led to rupturing of thrust faults at the boundary between the Lorestan mountain arc and Dezful sedimentary basin. The main shock and strongest aftershock occurred on north-sloping planes and contributed to the observed surface deformation. The results of seismological and geodetic inversions showed that the earthquake occurred mainly or completely within the thick sedimentary sequence. The relationship between the azimuth of the thrust slip vectors and terrain in the region implies that gravitational driving forces played an important role in this deformation and that the Lorestan arc is composed of weaker material compared to the Dezful basin (*Copley et al.*, 2015).

The focal mechanism of this strong earthquake satisfies the type of stress state established by us from the sets of focal mechanisms.

Table 2. Strongest earthquakes within spatial samplings IR1–IR12 in Iran, 1970–2020

Region	Date, time	Coordinates		M_W	Orientation of principal axes of mechanism						μ_M	Source
		N	E		T		B		P			
					Az	α	Azm	α	Az	α		
IR1	November 12, 2017 18:18:17	34.99	45.84	7.3	018	54	125	12	223	33	+0.0374	NEIC
		34.83	45.84	7.4	022	51	122	08	218	38	–0.0066	GCMT
IR_1-2	August 18, 2014 02:32:05	32.63	47.52	6.1	029	56	121	01	212	34	+0.1197	NEIC
		32.59	47.53	6.2	005	68	119	09	212	20	+0.2162	GCMT
IR2	January 12, 2013 03:25:05	31.75	50.95	5.2	103	48	277	42	010	03	+0.4984	GCMT
IR3	March 1, 1994 03:49:00	29.10	52.62	6.0	095	01	322	89	185	01	–0.2464	NEIC
		28.75	52.42	6.0	091	01	190	84	001	06	–0.3285	GCMT
IR4	September 10, 2008 11:00:34	26.74	55.83	6.1	221	65	047	24	316	02	+0.2001	NEIC
		26.65	55.72	6.2	007	75	246	08	154	12	+0.3790	GCMT
IR5	April 18, 2018 10:58:51	27.79	62.05	7.0	291	04	127	85	021	01	–0.2987	NEIC
		27.94	62.04	6.7	335	04	244	15	081	74	–0.0540	GCMT
IR6	May 10, 1997	33.82	59.81	7.3	108	03	330	86	198	03	+0.0758	NEIC
	07:57:29	33.58	60.02	7.2	113	05	341	83	203	05	+0.0735	GCMT
IR7	February 4, 1997 10:37:47	37.66	57.29	6.5	098	04	259	86	008	01	+0.2237	NEIC
		37.82	57.50	6.5	282	00	014	77	192	13	+0.0379	GCMT
IR8	August 27, 2008 19:23:50	35.49	54.47	5.8	066	03	000	90	335	11	0.0000	NEIC
		35.53	54.49	5.8	076	07	313	78	168	10	–0.0019	GCMT
IR9	June 20, 1990 21:00:10	36.96	49.41	7.3	183	47	321	35	067	22	–0.1093	NEIC
		36.95	49.52	7.3	163	34	325	54	067	09	–0.3608	GCMT
IR10	January 12, 2001 15:31:44	33.24	56.93	6.0	005	54	123	19	224	29	–0.0472	GCMT
IR11	August 11, 2008 12:23:18	38.33	46.83	6.4	219	07	099	77	311	11	+0.1197	NEIC
		38.31	46.80	6.5	040	11	231	79	130	02	+0.2162	GCMT
IR12	December 12, 2000 17:11:06	39.57	54.80	7.0	323	59	099	23	198	19	+0.0049	NEIC
		39.60	54.87	7.0	323	60	098	23	197	19	–0.1805	GCMT

Earthquake date and time are for NEIC solutions. The orientation of the principal axes—azimuths (Az) and angles of inclination with the horizon (α)—is given for CMT solutions. μ_M are the Lode–Nadai coefficients calculated from the eigenvalues of the CMT tensor matrix.

IR2. In this sampling, we failed to find a strong earthquake with $M_W \geq 6$; therefore, we included the earthquake of January 12, 2013, with $M_W = 5.2$ as the strongest in the last 50 years. The focal mechanism of this earthquake shows predominant lateral compression ($\mu_M \approx +0.5$) on inclined thrust planes. It also almost completely corresponds to the type of average mechanism established by us (see Table 1). The orientation of the principal axes of compression nearly coincides in both cases: their azimuths are in 10°–28°, and their inclinations to the horizon are 3°–5° (Tables 1, 2). The Lode–Nadai coefficients are also close: $\mu_M \approx +0.5$ for the strong earthquake focal mechanism and $\mu_M \approx +0.4$ for the average mechanism established by us based on a set of 176 focal mechanisms of medium-strength earthquakes ($4.4 \leq M_W \leq 6.5$). The relatively large Lode–Nadai coefficients compared to their values within the IR1 sampling can be considered evidence of increased lateral compression within the Zagros fold–thrust belt moving from northwest to southeast.

IR3. This sampling contains a strong earthquake on March 1, 1994, with $M_W = 6.0$. Its focal mechanism is close to shear with a significant lateral tensile component on subvertical planes ($\mu_M \approx -0.3$). The average

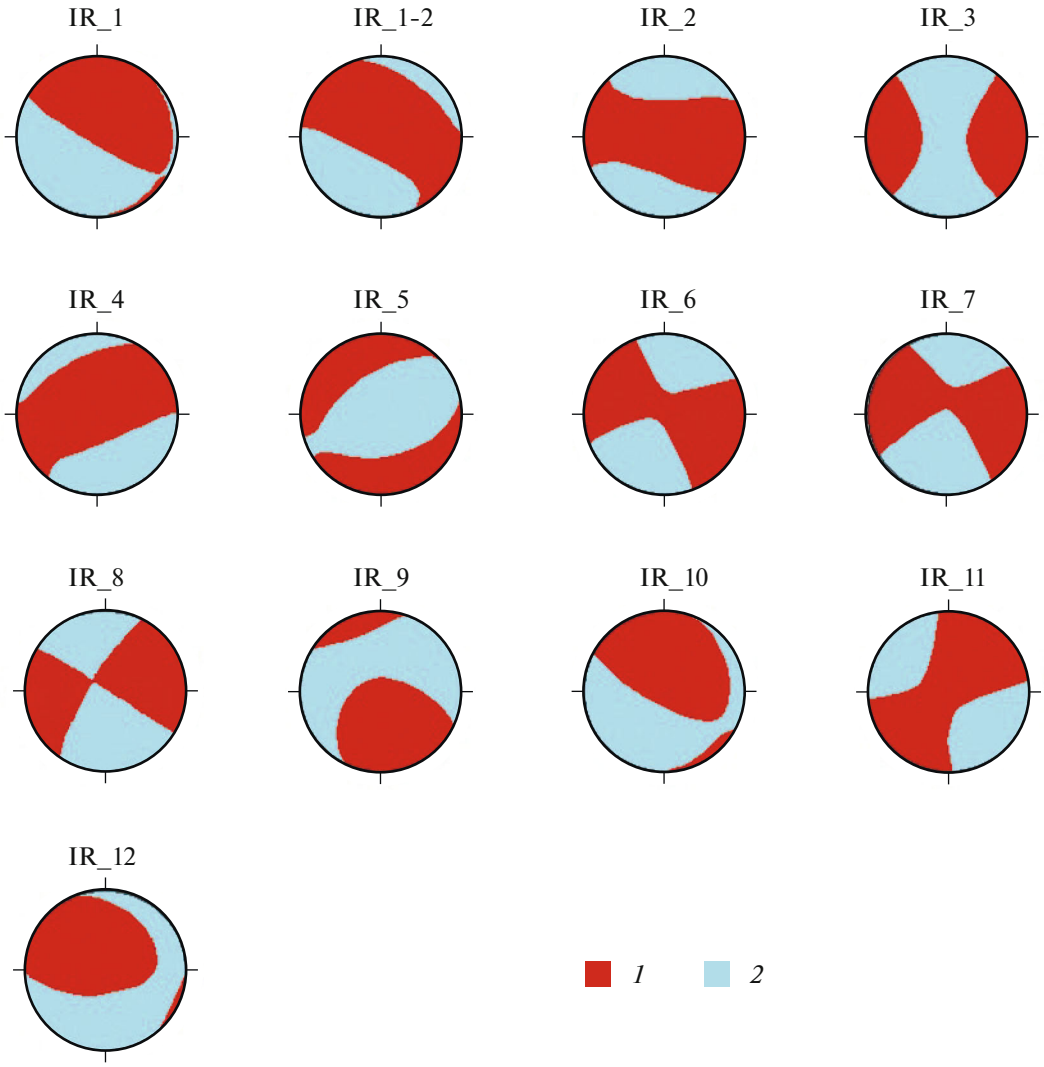

Fig. 7. Plots of CMT solutions for strongest earthquakes in last 50 years within samplings IR1–IR12. *1*, Extension zone; *2*, compression zone.

mechanism established by us from a set of 103 focal mechanisms of medium-strength earthquakes ($4.4 \le M_W \le 6.1$) is represented as thrust with a significant lateral compression component ($\mu_M \approx +0.38$). The orientation of the principal axes of compression and extension also differs: whereas the subhorizontal compression axes in both cases differ by an azimuth of 10° (see Tables 1 and 2), the axis of extension for the average mechanism assumes an almost vertical inclination to the horizon compared to the horizontal axis of compression at the strong earthquake focal mechanism. Thus, it can be argued that there are significant differences in the compared mechanisms. If the type of average mechanism in the IR3 sampling continues to correspond to predominant thrust formation within the Zagros fold–thrust belt throughout its entire length from sampling IR1 to sampling IR3, showing only some rotation of the subhorizontal axis of compression from diagonal to submeridional, then the focal mechanism of the strong earthquake with $M_W = 6.0$ within sampling IR3 instead corresponds to strike-slip movement, obliquely cutting through the strike of the Zagros Mountains.

IR4. The earthquake of September 10, 2008, with $M_W = 5.9–6.0$ occurred near Qeshm Island in the Persian Gulf. Its focal mechanism corresponded to thrust with a significant lateral compression component ($\mu_M \approx +0.38$), when the subhorizontal axis of compression is oriented at an azimuth of 154°. It was followed by a powerful series of aftershocks of five events with $M_W = 5.0–5.4$; almost all of them had focal mechanisms identical to that of the main shock.

Qeshm Island is located in the Persian Gulf in the southeastern part of the Zagros fold–thrust belt and is covered mainly with Neogene marble, sandstone, and

limestone, folded into two main anticlines extending from northeast to southwest (*Nissen et al.,* 2010). Although no major fault traces have been observed on this island, it has experienced high historical and recent seismic activity.

The following interesting feature of seismicity in this region is noted. Relatively numerous weak earthquakes occurred here long before the onset of the strong earthquake at depths of 2–4 km. Conversely, the aftershocks of the strong earthquake of September 10, 2008, are concentrated in the vicinity of the plane plunging southeast in the 10–20 km depth interval (Nissen et al., 2010). The hypocenter of the main shock was at a depth of 8 km in the upper part of the aftershock cluster. It can be assumed that this inclined earthquake cluster marks the working plane of the focal mechanism of the main shock (Fig. 7, Table 2). The seismogenic rupture did not reach the surface; it is suggested that it was hindered by the overlying weak Proterozoic Hormuz salt layer, separating the sedimentary cover in the 0–4 km depth interval from the crystalline basement. Thus, it can be suggested that the Hormuz salt forms an important regional barrier to seismogenic ruptures when strong earthquakes occur (*Nissen et al.,* 2010).

The emerging differences between the compared mechanisms for a strong earthquake and sets of focal mechanisms of 103 medium-strength earthquakes ($4.4 \le M_W \le 6.2$) in sampling IR3 continue in sampling IR4: if a strong earthquake causes a stress state of predominant subhorizontal compression at an azimuth of 154°, then for the average mechanism, the horizontal axis of compression is oriented at a significantly different azimuth (190°). These differences can be attributed to the complexity of the geological structure of the Oman region representing this sampling; here the longitudinal NW–SE trending faults and folds of the Zagros bend sharply to the northeast–southwest strike. The latter also corresponds to one of the slip planes in the focal mechanism of the strong earthquake.

IR5. April 18, 1983, in the Makran region, near the Pakistani–Iranian border, there was a strong earthquake with $M_W = 6.7–7.0$ (with a seismic moment $M_0 = 1.2 \times 10^{19}$ Nm) (Laane and Chen, 1989). This earthquake is the only such strong event in the area since the great Makran earthquake ($M_W = 8.0$) in 1945. The centroid solution shows normal faulting; the great Makran earthquake of 1945 had a similar focal mechanism (Laane and Chen, 1989). In contrast to all other strong earthquakes of Iran considered here, the earthquake of April 18, 1983, occurred at a depth of about 65 km. The great Makran earthquake of 1945 occurred at approximately the same depth. The large depth of these earthquakes confirms the hypothesis that there is a collision zone in the Makran region in the form of plunging of the Arabian Plate under Eurasia (Nilforoushan et al., 2003; Masson et al., 2007).

The normal-fault focal mechanism, atypical of other strong earthquakes in Iran, is interpreted in (Laane and Chen, 1989) as evidence of normal faulting in the relatively old subducting Arabian Plate. The axis of subhorizontal extension corresponding to the normal-fault focal mechanism of the strong earthquake is oriented at an azimuth 335°. Approximately at the same azimuth (322°), the subhorizontal axis of extension of the average mechanism is also oriented at $\mu_M \approx -0.4$. Thus, it can be stated that there is a certain correspondence between the focal mechanism of the strong earthquake, the average mechanism for the sets of focal mechanisms of relatively weak earthquakes, and the tectonics of the Makran region.

IR6. A destructive earthquake with $M_W = 7.2–7.3$ occurred on May 10, 1997, near the settlement of Zirkuh in the northeastern part of the Lut block and led to the formation of a NNW–SSE-trending surface dextral strike-slip fault with a length of 125 km. The fault was located directly within the Abiz Fault in the Sistan suture zone on the northeastern shoulder of the submeridional right-hand strike-slip system that bounded the rigid Lut block from the east. The seismogenic rupture was the longest of all known Iranian earthquake ruptures.

Studies (Sudhaus and Jonsson, 2011; Ansari, 2021) show that during this earthquake, with a predominantly strike-slip displacement, there was a distinct change in the style of displacement along its rupture. Thus, in the north, a significant thrust component is found on a seismogenic fault plunging in the western direction, along which mainly shear displacement occurs. At the southern end of the seismogenic fault, the thrust orientation changes to displacement along the eastward inclined fault plane. The central part of the fault is vertical and is almost pure dextral shear.

This inhomogeneous slip distribution along the fault indicates the existence of two areas (north and south) with low slip, located near significant changes in the structure of the Abiz fault. These structural changes in the fault configuration are also confirmed by field geological observations. Therefore, these structural complexities really exist and they slow down slippage of the seismogenic rupture along the Abiz fault. The described changes in the style of seismogenic displacement along the Abiz fault were observed both in coseismic surface ruptures and in geomorphology. The average coseismic surface displacements were approximately 2 m, which corresponds to a static drop in stress of only 5 bar (0.5 MPa).

In this case, there is an almost complete correspondence between the shear focal mechanism of the strong earthquake and fault tectonics at the northeastern end of the rigid Lut block. At the same time, according to mean mechanism estimates, uniaxial compression predominated ($\mu_M = 0.7$) at an azimuth of 44° (Table 1). The orientation of this compression differs by 21° from the orientation of the axis of subho-

rizontal compression (Azm = 23°) in the strong earthquake focal mechanism. This difference is fundamental, since, according to tectonic concepts, the rigid Lut block is being squeezed out as a whole along the fault zones bounding it from the west and east, submeridionally to the north. We do not yet understand the reason for this discrepancy.

IR7. On February 4, 1997, an earthquake with $M_W = 6.4–6.5$ occurred as a result of an almost pure dextral strike-slip motion with an offset of 0.5–1.0 m, which ruptured a 15 km long fault section with a strike of ~340° at its northern end, changing to ~320° at its southern end. This rotation of the seismogenic fault observed on the surface is distinctly visible on satellite images and corresponds to similar rotation of a tectonic fault known here (Hollingsworth et al., 2006). The seismogenic fault nearly coincides with the southern end of this tectonic fault.

The stress state in the vicinity of the strong earthquake, estimated by us from the set of focal mechanisms for 20 earthquakes with $M_W = 4.8–6.0$, is characterized by intense subhorizontal compression ($\mu_M \approx +0.66$) at an azimuth of 212°, close to the azimuth of the axis of subhorizontal compression (192°) in the source of the strong earthquake. Thus, it can be assumed that the seismogenic shear at the source of this strong earthquake occurred in a setting of intense lateral compression on the subvertical fault plane.

IR8. The earthquake of August 27, 2010, with $M_W = 5.8–5.9$ occurred in Koh-Zar in northeast Iran in the Eastern Alborz. In the vicinity of the epicenter, a strong earthquake had struck earlier in 1953, which also caused significant damage and destruction. A macroseismic survey of the August 27, 2010 earthquake showed that the highest shaking intensity VII (MMI) was observed in Koh-Zar. The earthquake was not associated with any significant surface fault, but as a result of it, coseismic folding of the exposed surface occurred (Shahvar and Zaré, 2013). It was reported that the source of this folding was a sinistral slip mechanism in the northeast–southwest direction. A regional strong-movements network, consisting of seven stations (SSA-2 accelerographs), located within 4–130 km from the epicenter of this earthquake, showed that the rupture propagated SW towards Koh-Zar (Shahvar and Zaré, 2013).

The focal mechanism of this strong earthquake is characterized by pure shear with orientation of the principal axes of compression and extension at azimuths of 168° and 76°, respectively. At the same time, the SSS in the vicinity of the strong earthquake, according to the set of focal mechanisms for 24 earthquakes with $M_W = 5.0–6.1$, is characterized by intense subhorizontal compression ($\mu_M \approx 0.4$) with the horizontal axis of compression at an azimuth of 10°.

IR9. The earthquake in Rudbar on June 20, 1990, is the first high-magnitude earthquake with 80 km dextral strike-slip motion in the western part of the Alborz fold–thrust mountain belt (*Gao and Wallace,* 1995). It was one of the largest and most destructive earthquakes that occurred in Iran during the instrumental period. The seismogenic surface rupture during this earthquake was approximately parallel to the Rudbar fault about 10 km north of it. The coseismic surface rupture that occurred on a previously unknown fault with little geomorphological expression showed unusually large vertical offset directed opposite the existing topography. Analysis of satellite images shows that the total sinistral displacement on the Rudbar fault is ~1 km. The observed sinistral displacements of river valleys by ~200 m along the Kashachal fault and up to ~1.5 km along the Kelishom fault, which are located at the eastern end of the Rudbar seismogenic fault, confirm its modern activity. Given the relatively small displacements, it should be assumed that the active sinistral strike-slip faults in the western part of the High Alborz fold–thrust belt can be much younger than the very onset of the deformation in the Alborz Mountains, dated ~5 Ma ago (Berberian and Walker, 2010).

The seismogenic rupture during the strong Rudbar earthquake of 1990 is one of three en echelon parallel sinistral faults observed here with signs of modern activity. The apparent sinistral displacements on the nearby Kelishom and Kashachal faults highlight them as potential eastward extensions of the active fault that formed during the Rudbar earthquake. Thus, these two faults are potential sources of future large earthquakes and should be the subject of further detailed studies.

The focal mechanism of this strong earthquake is characterized by subhorizontal compression at an azimuth of 67°. This compression results in shear displacement along the newly formed fault, the strike of which corresponds to the existing fault system here. At the same time, the SSS in the vicinity of the strong earthquake, according to the set of focal mechanisms for 31 earthquakes with $M_W = 4.4–6.5$, is characterized by almost pure thrust formation ($\mu_M \approx 0$) on the horizontal axis of compression at an azimuth of 25°. This direction lies approximately across the strike of the Western Alborz (see Fig. 1), which can be considered evidence of satisfactory agreement between assessment of the SSS type based on the sets of focal mechanisms of medium-strength earthquakes and modern orogeny within this part of the Alborz Mountains, one element of which can be shear destruction, realized in the sources of strong earthquakes.

IR10. The strongest earthquake in the last 50 years for the Iranian central block on January 12, 1980, with $M_W = 6.0$ can be characterized as thrust ($\mu_M \approx 0.0$) with the orientation of the axis of compression slightly inclined to the horizon at an azimuth of 224° (see Table 2). The SSS reconstructed for the Iranian central block is characterized by intense subhorizontal compression ($\mu_M \approx 0.64$) in the meridional direction

(Azm = 199°). This subhorizontal compression setting corresponds to tectonic ideas about intense meridional compression of this area during continental collision of the Arabian and Eurasian plates.

IR11. On August 11, 2012, an earthquake with $M_W = 6.4$ occurred at a depth of about 9 km, followed by another earthquake with $M_W = 6.3$ at a depth of 16 km. The parameters of the strongest of them are given in Table 2. The events occurred with a time interval of 11 min and distance interval of 6 km, which led to a surface rupture about 12 km in length (Esmaeili and Zareh, 2014; Donner et al., 2015). Despite the fact that the nearest tectonic fault zone here is the active Tabriz fault, the epicenters of these strong earthquakes were at a significant distance (~50 km) from the fault, so they were not caused by slip along the Tabriz fault. The fault closest to the epicenter of this strong double earthquake is sublatitudinally trending secondary dextral South Akhara strike-slip.

The focal mechanism of the strongest event is consistent with dextral shear along this fault in the sublatitudinal direction, established by field observations (Kalantari and Parsizadeh, 2012). However, the second shock demonstrates a significant thrust component. The analysis in (Kalantari and Parsizadeh, 2012) shows that the neighboring North Tabriz fault, which accommodates up to 7 mm/year of dextral shear, does not compensate for the entire shear deformation, and this part is compensated further to the north, in particular, on the sublatitudinally trending dextral South Akhara strike-slip fault identified in (Kalantari and Parsizadeh, 2012; Esmaeili and Zareh, 2014; Donner et al., 2015). These results indicate a complex (thrust and shear) spatiotemporal style of deformation in the vicinity of the strong earthquake of August 11, 2012, overprinted on an older thrust deformation.

The focal mechanism of this strong earthquake is represented by shear ($\mu_M \approx 0.2$, which is close to zero) with the subhorizontal principal axes of compression and extension oriented at azimuths of 130° and 40°, respectively. The strike of the working plane of fault displacement is close to the sublatitudinal strike of the minor dextral South Akhara Fault. The SSS in the vicinity of the strong earthquake, established from sets of focal mechanisms of medium-strength earthquakes, is characterized by transpression ($\mu_M \approx 0.4$) with orientation of the subhorizontal axis of compression at an azimuth of 159°, which differs by only 29° from that for the strong earthquake focal mechanism. Therefore, it can be stated that in this region there is a good correspondence between the reconstructed stress state, modern tectonics, and nature of seismogenic displacement in the source of the strongest earthquake for this territory.

IR12. In the focal mechanism of the strongest earthquake in this region on December 6, 2000, with $M_W = 7.0$, one of the two possible slip planes is oriented in the sublatitudinal direction at angles of inclination of 19° and 60°, respectively, to the horizon of the axes of compression and extension. For a Lode–Nadai coefficient of $\mu_M \approx -0.2$, this plane can be interpreted as an inclined incision plane. The SSS, reconstructed from medium-strength earthquakes, is also characterized by a pronounced incision ($\mu_M \approx -0.2$) at an inclination of the principal axes of compression and extension oriented submeridionally at angles of 40° and 49°, respectively, to the horizon. Given that the earthquake occurred at the eastern end of the submarine Absheron–Balkhan basement high with significant uplift of the northern side with respect to the southern, we can suggest that the data presented here on the nature of the SSS and type of slip during the strongest earthquake in this region fit the modern tectonics.

DISCUSSION

Iran is an extremely interesting region in terms of seismotectonics. Here, according to modern tectonic concepts, Iran hosts one of the largest zones of continental collision between the Arabian and Eurasian plates. The nature of deformation of this zone is heterogeneous due to the combined collisional and continental tectonics here. This heterogeneity also gives rise to a heterogeneous spatial structure of the seismicity in the territory under consideration: here, along with extremely highly seismic areas, vast areas with almost complete absence of strong seismicity are distinguished.

The most seismotectonically homogeneous structure is the Zagros fold–thrust belt, represented in our study by spatial samplings IR1–IR4. It is within the Zagros belt that the majority of deformation caused by the collision of lithospheric plates occurs as intense thrust formation (in the azimuthal sector 19°–31° according to our estimates) across the strike of a NW–SE-oriented linear fault system, bounded in the south by the Zagros frontal fault (ZFF), and in the north, by the Main Zagros Fault (MZT). It results mainly from shortening of the fold belt across its strike with the formation of the Zagros Mountains.

The territory of the fold belt, bounded by the indicated large thrusts, is covered by the largest surface deformation rates (~5–10 mm/year) according to GPS observations (Tavakoli et al., 2008). Further north, within the Central Iran Plateau (IR10), internal deformation sharply decreases to less than 2 mm/year (Vernant et al., 2004a; Tavakoli et al., 2008).

Within the fold belt, a large number of strongest earthquakes with magnitudes $M_W \approx 6.5–7$ have occurred. The seismic movements considered here in the sources of some of these earthquakes match the type of SSS established by us from a total set of about 500 focal mechanisms of medium-strength events ($4.4 \le M_W \le 6.5$). There is a certain overall increase in

the intensity of subhorizontal compression moving from the Western to Eastern Zagros.

In the Oman region (sampling IR4), a change in the overall thrust formation regime is noted. Here, the longitudinal NW–SE-oriented faults and folds of the Zagros belt bend sharply to the northeast–southwest. The latter also corresponds to one of the slip planes in the focal mechanism of the strongest earthquake known here with $M_W = 6.2$. In addition, here, the orientation of the stress state of subhorizontal compression deviates from the general regularity to submeridional (Azm = 190°).

This change is most likely due to the transition from fold–thrust orogeny in the Zagros belt to a subduction regime in the Makran region (IR5). It is here that we have established a type of stress state in the form of subhorizontal tension ($\mu_M = -0.4$) at an azimuth of 322°. The principal axis of extension in the fault focal mechanism of the strongest earthquake during the considered time frame($M_W = 6.7–7.0$) was oriented at approximately the same azimuth (335°). A similar normal-fault focal mechanism is interpreted in (Laane and Chen, 1989) as evidence of normal faulting in the relatively old subducting Arabian Plate. Such a sharp change in the tectonic regime is also indicated by numerous geological and tectonic evidence of modern subduction of the Arabian Sea floor under the coast of Makran (see, e.g., (Jackson and McKenzie, 1984; Maggi et al., 2000)). A significant amount of stretching at approximately the same azimuth was established in the west of the Makran region and in the Gulf of Oman based on GPS observations (Khorrami et al., 2019) (see Fig. 4).

Geological structures on opposite sides of the meridional Kazerun–Borodzhan fault zone and its further southward continuation in the form of the Minab–Zendan fault zone have been crushed during collisions of different intensity. Thus, according to modern GPS measurements (Tatar et al., 2002; Vernant et al., 2004b; Hessami et al., 2006; Walpersdorf et al., 2006; Tavakoli et al., 2008), the Western Zagros are moving at a rate of ~4 ± 2 mm/year in the direction of 12 ± 8° NNW, and the Eastern Zagros, at a rate of ~9 ± 2 mm/year, is moving in the direction of 7 ± 5° NNE (Hessami et al., 2006; Tavakoli et al., 2008). To some extent, this increase in crushing intensity can also be attributed to the Lut block (IR6), within which we found predominant intense subhorizontal compression ($\mu_M = +0.7$) at an azimuth of 44°. At the same time, this direction hardly agrees with tectonic concepts, according to which the rigid Lut block is being squeezed out to the north in a submeridional direction as a single whole along the fault zones bounding it from the west and east. We do not yet understand the reason for this discrepancy.

North of the Main Zagros Fault (MZT in Fig. 1), in the central part of Iran, is the Iranian Plateau (IR10), within which fold–thrust deformation characteristic of the Zagros belt all but disappears; according to GPS measurements, it was less than 2 mm/year (Vernant et al., 2004b; Tavakoli et al., 2008). This absence of deformation is accompanied by the almost complete absence of seismicity within the Iranian Plateau (see, e.g., Fig. 2), which allows many researchers to consider it as a rigid, undeformable block of continental lithosphere.

North of the Iranian Plateau is the arcuate Alborz fold–thrust belt (IR8 and IR9), the lower point of which lies at 52.5° E, and its eastern (IR8) and western (IR9) branches extend, respectively, to the northeast at an azimuth of 80° and to the northwest at an azimuth of 290°, skirting the Caspian depression from the south.

Combined with submeridional convergence of the Central Iranian Plateau, the southwestward movement of the South Caspian Basin with respect to Central Iran leads to a transpressional regime with submeridional compression in the Alborz range. This transpression must have started 3–7 Ma ago (Ritz et al., 2006). Until that time, the sinistral movements that prevailed, observed in the field along faults parallel to the strike of the Alborz range, indicate that the mountains were deformed relatively rigidly, resulting in a submeridional compression regime in the stable South Caspian zone to the north (Axen et al., 2001; Jackson et al., 2002; Allen et al., 2003). Sets of parallel shear and thrust faults in the Alborz region can operate together such that the total slip and shortening can be combined to calculate the overall north–south convergence in this region (Talebian and Jackson, 2002).

Analysis of GPS data shows that within the Alborz mountains, there is significant (compared to the Iranian Plateau) shortening from north to south at a rate of 5 ± 2 mm/year with a smaller (at a rate of 4 ± 2 mm/year) value of sinistral shear (Vernant et al., 2004b). Our estimates of the SSS also showed predominant thrust formation within the entire Alborz mountain belt with a significantly larger compression component ($\mu_M = +0.4$) in its eastern part (IR8) compared to the western one ($\mu_M \approx 0$); at the same time, shear deformation occurs in the sources of the strong earthquakes considered here in the eastern and western parts of Alborz. Therefore, it is believed that sinistral shear displacements on en echelon subparallel faults are potential sources of future earthquakes of large magnitude in this region. And the fact that such events have already taken place here quite frequently is evidenced, e.g., in Fig. 2.

Further west, convergence of the Arabian and Eurasian plates leads to pushing of the Anatolian block to the west, bounded in the north by the dextral North Anatolian fault, and in the south by the sinistral South Anatolian fault (Authemayou et al., 2009). Apparently, this pushing process continues further north within the Talesh mountain range (IR11). This is partly confirmed by the dextral shear displacement

along the sublatitudinal North Tabriz fault (NTF in Fig. 1), the main tectonic element in this region. The shear displacement along the North Tabriz fault is opposite the displacement along faults close in strike (280°) in the neighboring Western Alborz range (IR9). Strike-slip faulting within the Talesh ridge is confirmed both by the mechanism of the strongest earthquake over the above period within sampling IR11 (see Table 2) and by the transpression regime established by us based on a set of 69 focal mechanisms of medium-strength events ($4.4 \le M_W \le 6.4$).

East of the Alborz range, in the Kopetdag range, the direction of transpression changes from submeridional in the Alborz range to the northeast. The existence of shortening across the Kopetdag range has been established by GPS observations (Zarifi et al., 2014; Khorrami et al., 2019) (cf. Fig. 4). It is believed that the tectonic forces in the Kopetdag range and Eastern Iran have the same origin (Walker and Jackson, 2004). Dextral strike-slip displacement along the Dorouneh fault (DF in Fig. 1), which bounds the rigid Lut block from the north, transfers subhorizontal compressive stress acting in the Lut block, according to our determinations ($\mu_M \approx +0.7$), farther north, and thus results in transverse shortening of the Kopetdag range. The stress state estimated by us in the Kopetdag range (IR7) is characterized by intense subhorizontal compression ($\mu_M = +0.66$) at an azimuth of 212°. The axis of maximum compression in the shear focal mechanism of the strongest earthquake ($M_W = 6.5$) in the last 50 years in the Kopetdag range is oriented at approximately the same azimuth (see Table 2). Thus, it can be suggested that this seismogenic shear occurred on a subvertical plane in a setting of intense lateral compression, established from geodetic, seismological, and tectonic data.

The submarine Absheron–Balkhan ridge (IR12), located in the extreme north of this territory, is an offshore continuation of the Caucasus to the east through the Caspian Sea. It formed on a basement high with significant uplift of the northern side with respect to the southern and separates the South Caspian from the North Caspian basin. At the same time, the South Caspian basin has relatively thin oceanic crust, while the North Caspian basin has thicker continental crust (Mangino and Priestley, 1998). The SSS of the Absheron–Balkhan submarine ridge, reconstructed from medium-strength earthquakes, is characterized by pronounced incision ($\mu_M \approx -0.2$) at an inclination of the principal axes of compression and extension oriented in the submeridional direction at angles to the horizon of 40° and 49°, respectively. The focal mechanism of the strongest earthquake for these areas in the past 50 years ($M_W = 7.0$) matches this type of stress state (see Table 2). The GPS observation data (see Fig. 4) show distinctly predominant compression across the strike of the underwater ridge (Khorrami et al., 2019), which determines the nearly meridional compressive regime of the Absheron–Balkhan basement high.

CONCLUSIONS

The paper is brief review of the currently existing ideas on the seismotectonic setting in the Earth's crust of Iran, which is generally experiencing intense compression in the northeast direction as a result of collision of the Arabian and Eurasian plates. The review also involves geodetic data in the form of modern GPS measurements of horizontal surface displacements in Iran.

The stress-strain state of the crust of Iran (construction of the average focal mechanism) was estimated based on data from a set of 945 focal mechanisms of medium-strength earthquakes ($4.4 \le M_W \le 6.5$) according to the ISC catalog that occurred from 1975 to 2020 within 12 spatial samplings. The focal mechanisms of the strongest earthquakes over the past 50 years (one such event in each of these samplings) are also considered.

The calculated parameters of the average mechanisms and focal mechanisms were compared both with each other and the surrounding tectonic setting and distribution of the strain rate vectors based on GPS observations. Satisfactory correspondence between all compared values was established. Differences in the type of deformation of the seismogenic layer of the crust of Iran in different regions are demonstrated.

Based on the results of the study, it can be stated that there is a satisfactory correspondence between deformations, stresses, and the location of the strongest earthquakes in the crust of Iran. This allows us to accept collision of the Arabian and Eurasian lithospheric plates as the main source of tectonic, geodetic, and seismological manifestations in Iran.

FUNDING

The study was carried out under the state task of the Schmidt Institute of Physics of the Earth, Russian Academy of Sciences (topic no. 0144-2019-0011).

CONFLICT OF INTEREST

The authors declare that they have no conflicts of interest.

REFERENCES

Allen, M.B., Ghassemi, M.R., Shahrabi, M., and Qorashi, M., Accommodation of late Cenozoic oblique shortening in the Alborz range, northern Iran, *J. Struct. Geol.*, 2003, vol. 25, no. 5, pp. 659–672. https://doi.org/10.1016/S0191-8141(02)00064-0

Allen, M.B., Jackson, J., and Walker, R., Late Cenozoic reorganization of the Arabia-Eurasia collision and the comparison of short-term and long-term deformation rates,

Tectonics, 2004, vol. 23, no. 2, p. TC2008.
https://doi.org/10.1029/2003TC001530

Allen, M.B., Kheirkhah, M., Emami, M.H., and Jones, S.J., Right-lateral shear across Iran and kinematic change in the Arabia–Eurasia collision zone, *Geophys. J. Int.*, 2011, vol. 184, no. 2, pp. 555–574.
https://doi.org/10.1111/j.1365-246X.2010.04874.x

Allen, M.B., Saville, C., Blanc, E.J.-P., Talebian, M., and Nissen, E., Orogenic plateau growth: Expansion of the Turkish-Iranian Plateau across the Zagros fold-and-thrust belt, *Tectonics*, 2013, vol. 32, no. 2, pp. 171–190.
https://doi.org/10.1002/tect.20025

Altamimi, Z., Rebischung, P., Métivier, L., and Collilieux, X., ITRF2014: A new release of the international terrestrial reference frame modeling nonlinear station motions, *J. Geophys. Res.*, 2016, vol. 121, no. 8, pp. 6109–6131.
https://doi.org/10.1002/2016JB013098

Ansari, S., Structural and stress heterogeneities along the 1997 Zirkuh earthquake fault, Eastern Iran, *Bull. Eng. Geol. Environ.*, 2021, vol. 80, no. 11, pp. 8319–8337.
https://doi.org/10.1007/s10064-021-02436-7

Authemayou, Ch., Bellier, O., Chardon, D., Benedetti, L., Malekzade, Z., Claude, Ch., Angeletti, B., Shabanian, E., and Abbassi, M.R., Quaternary slip-rates of the Kazerun and the Main Recent Faults: Active strike-slip partitioning in the Zagros fold-and-thrust belt, *Geophys. J. Int.*, 2009, vol. 178, no. 1, pp. 524–540.
https://doi.org/10.1111/j.1365-246X.2009.04191.x

Axen, G.J., Lam, P.S., Grove, M., Stockli, D.F., and Hassanzadeh, J., Exhumation of the west-central Alborz Mountains, Iran, Caspian subsidence, and collision-related tectonics, *Geology*, 2001, vol. 29, no. 6, pp. 559–562.
https://doi.org/10.1130/0091-7613(2001)029<0559:EOTWCA>2.0.CO;2

Bachmanov, D.M., Zelenin, E.A., Kozhurina, A.I., and Trifonov, V.G., Using the active faults of Eurasia database for solving tectonic problems, *Geodin. Tektonofiz.*, 2019, vol. 10, no. 4, pp. 971–993.
https://doi.org/10.5800/GT-2019-10-4-0453

Bayer, R., Chery, J., Tatar, M., Vernant, Ph., Abbassi, M., Masson, F., Nilforoushan, F., Doerflinger, E., Regard, V., and Bellier, O., Active deformation in Zagros–Makran transition zone inferred from GPS measurements, *Geophys. J. Int.*, 2006, vol. 165, no. 1, pp. 373–381.
https://doi.org/10.1111/j.1365-246X.2006.02879.x

Berberian, M. and Walker, R., The Rudbār M_w = 7.3 earthquake of 1990 June 20; seismotectonics, coseismic and geomorphic displacements, and historic earthquakes of the western 'High-Alborz', Iran, *Geophys. J. Int.*, 2010, vol. 182, no. 3, pp. 1577–1602.
https://doi.org/10.1111/j.1365-246X.2010.04705.x

Copley, A., Karasozen, E., Oveisi, B., Elliott, J.R., Samsonov, S., and Nisen, E., Seismogenic faulting of the sedimentary sequence and laterally variable material properties in the Zagros Mountains (Iran) revealed by the August 2014 Murmuri (E. Dehloran) earthquake sequence, *Geophys. J. Int.*, 2015, vol. 203, no. 2, pp. 1436–1459.
https://doi.org/10.1093/gji/ggv365

DeMets, C., Gordon, R.G., Argus, D.F., and Stein, S., Effect of recent revisions to the geomagnetic reversal timescale on estimates of current plate motions, *Geophys. Res. Lett.*, 1994, vol. 21, no. 20, pp. 2191–2194.
https://doi.org/10.1029/94GL02118

Djamour, Y., Vernant, Ph., Bayer, R., Nankali, H.R., Ritz, J.-F., Hinderer, J., Hatam, Y., Luck, B., Le Moigne, N., Sedighi, M., and Khorrami, F., GPS and gravity constraints on continental deformation in the Alborz mountain range, Iran, *Geophys. J. Int.*, 2010, vol. 183, no. 3, pp. 1287–1301.
https://doi.org/10.1111/j.1365-246X.2010.04811.x

Djamour, Y., Vernant, Ph., Nankali, H.R., and Tavakoli, F., NW Iran-eastern Turkey present-day kinematics: Results from the Iranian permanent GPS network, *Earth Planet. Sci. Lett.*, 2011, vol. 307, nos. 1–2, pp. 27–34.
https://doi.org/10.1016/j.epsl.2011.04.029

Donner, S., Ghods, A., Krüger, F., Rößler, D., Landgraf, A., and Ballato, P., The Ahar-Varzeghan earthquake doublet (Mw 6.4 and 6.2) of 11 August 2012: Regional seismic moment tensors and a seismotectonic interpretation, *Bull. Seismol. Soc. Am.*, 2015, vol. 105, pp. 791–807.

Engdahl, E.R., Jackson, J.A., Myers, S.C., Bergman, E.A., and Priestley, K., Relocation and assessment of seismicity in the Iran region, *Geophys. J. Int.*, 2006, vol. 167, no. 2, pp. 761–778.
https://doi.org/10.1111/j.1365-246X.2006.03127.x

Esmaeili, B., Almasian, M., and Zare, M., Dating of South Ahar Fault seismic activity by thermo lominesense with regard to August 11th earthquake, *Second European Conference on Earthquake Engineering and Seismology*, Istanbul, 2014.

Feng, W., Samsonov, S., Almeida, R., Yassaghi, A., Li, J., Qiu, Q., Li, P., and Zheng, W., Geodetic constraints of the 2017 M_w 7.3 Sarpol Zahab, Iran earthquake and its implications on the structure and mechanics of the Northwest Zagros thrust-fold belt, *Geophys. Res. Lett.*, 2018, vol. 45, no. 14, pp. 6853–6861.
https://doi.org/10.1029/2018GL078577

Frohling, E. and Szeliga, W., GPS constraints on interpolate locking within Makran subduction zone, *Geophys. J. Int.*, 2016, vol. 205, no. 1, pp. 67–76.
https://doi.org/10.1093/gji/ggw001

Gao, L. and Wallace, T.C., The 1990 Rudbar-Tarom Iranian earthquake sequence: Evidence for slip partitioning, *J. Geophys. Res.*, 1995, vol. 100, no. B8, pp. 15317–15332.
https://doi.org/10.1029/95JB00320

Hessami, K., Nilforoushan, F., and Talbot, C., Active deformation within the Zagros Mountains deduced from GPS measurements, *J. Geol. Soc.*, 2006, vol. 163, no. 1, pp. 143–148.
https://doi.org/10.1144/0016-764905-031

Hollingsworth, J., Jackson, J., Walker, R., Gheitanchi, M.R., and Bolourchi, M.J., Strike-slip faulting, rotation, and along-strike elongation in the Kopeh Dagh mountains, NE Iran, *Geophys. J. Int.*, 2006, vol. 166, no. 3, pp. 1161–1177.
https://doi.org/10.1111/j.1365-246X.2006.02983.x

Horton, B.K., Hassanzadeh, J., Stockli, D.F., Axen, G.J., Gillis, R.J., Guest, B., Amini, A., Fakhari, M.D., Zamanzadeh, S.M., and Grove, M., Detrital zircon provenance of Neoproterozoic to Cenozoic deposits in Iran: Implications for chronostratigraphy and collisional tectonics, *Tectonophysics*, 2008, vol. 451, nos. 1–4, pp. 97–122.
https://doi.org/10.1016/j.tecto.2007.11.063

International Seismological, Centre. http://www.isc.ac.uk/registries/search/. Cited December 4, 2021.

Jackson, J. and McKenzie, D., Active tectonics of the Alpine–Himalayan Belt between western Turkey and Pakistan, *Geophys. J. Int.*, 1984, vol. 77, no. 1, pp. 185–264. https://doi.org/10.1111/j.1365-246X.1984.tb01931.x

Jackson, J., Priestley, K., Allen, M., and Berberian, M., Active tectonics of the South Caspian Basin, *Geophys. J. Int.*, 2002, vol. 148, no. 2, pp. 214–245. https://doi.org/10.1046/j.1365-246X.2002.01588.x

Kalantari, A. and Parsizadeh, F., The $M_w = 6.4$ and $M_w = 6.3$ Iran earthquakes of August 11, 2012, EERI Special Earthquake Report, 2012.

Khorrami, F., Vernant, Ph., Masson, F., Nilfouroushan, F., Mousavi, Z., Nankali, H., Saadat, S.A., Walpersdorf, A., Hosseini, S., Tavakoli, P., Aghamohammadi, A., and Alijanzade, M., An up-to-date crustal deformation map of Iran using integrated campaign-mode and permanent GPS velocities, *Geophys. J. Int.*, 2019, vol. 217, no. 2, pp. 832–843. https://doi.org/10.1093/gji/ggz045

Koronovskii, N.B., Bryantseva, G.V., Arkhipov, E.V., and Anisimova, O.V., Structural-geomorphological analysis and seismicity of Iranian region, *Byull. Mosk. O-va. Ispyt. Prir. Otd. Geol.*, 2017, vol. 92, no. 3, pp. 12–22.

Laane, J.L. and Chen, W.-P., The Makran earthquake of 1983 April 18: A possible analogue to the Puget Sound earthquake of 1965?, *Geophys. J. Int.*, 1989, vol. 98, no. 1, pp. 1–9. https://doi.org/10.1111/j.1365-246X.1989.tb05509.x

Lukk, A.A. and Rebetskii, Yu.L., Modern geodynamics and focal mechanisms of earthquakes in the neighborhood of Bushehr NPP, *Geofiz. Protsessy Biosfera*, 2018, vol. 17, no. 3, pp. 90–108. https://doi.org/10.21455/GPB2018.3-6

Maggi, A., Jackson, J.A., Priestley, K., and Baker, C., A reassessment of focal depth distributions in southern Iran, the Tien Shan and northern India: do earthquakes really occur in the continental mantle?, *Geophys. J. Int.*, 2000, vol. 143, no. 3, pp. 629–661. https://doi.org/10.1046/j.1365-246X.2000.00254.x

Mangino, S. and Priestley, K., The crustal structure of the southern Caspian region, *Geophys. J. Int.*, 1998, vol. 133, no. 3, pp. 630–648. https://doi.org/10.1046/j.1365-246X.1998.00520.x

Masson, F., Chéry, J., Hatzfeld, D., Martinod, J., Vernant, P., Tavakoli, F., and Ghafory-Ashtiani, M., Seismic versus aseismic deformation in Iran inferred from earthquakes and geodetic data, *Geophys. J. Int.*, 2005, vol. 160, no. 1, pp. 217–226. https://doi.org/10.1111/j.1365-246X.2004.02465.x

Masson, F., Djamour, Y., Van Gorp, S., Chéry, J., Tatar, M., Tavakoli, F., Nankali, H., and Vernant, P., Extension in NW Iran driven by the motion of the South Caspian Basin, *Earth Planet. Sci. Lett.*, 2006, vol. 252, nos. 1–2, pp. 180–188. https://doi.org/10.1016/j.epsl.2006.09.038

Masson, F., Anvari, M., Djamour, Y., Walpersdorf, A., Tavakoli, F., Daignieres, M., Nankali, H., and Van Gorp, S., Large-scale velocity field and strain tensor in Iran inferred from GPS measurements: new insight for the present-day deformation pattern within NE Iran, *Geophys. J. Int.*, 2007, vol. 170, no. 1, pp. 436–440. https://doi.org/10.1111/j.1365-246X.2007.03477.x

Masson, F., Lehujeur, M., Ziegler, Y., and Doubre, C., Strain rate tensor in Iran from a new GPS velocity field, *Geophys. J. Int.*, 2014, vol. 197, no. 1, pp. 10–21. https://doi.org/10.1093/gji/ggt509

Mousavi-Bafrouei, S.H. and Mahani, A.B., A comprehensive earthquake catalogue for the Iranian Plateau (400 B.C. to December 31, 2018), *J. Seismol.*, 2020, vol. 24, no. 3, pp. 709–724. https://doi.org/10.1007/s10950-020-09923-6

Mousavi, Z., Walpersdorf, A., Walker, R.T., Tavakoli, F., Pathier, E., Nankali, H., Nilfouroushan, F., and Djamour, Y., Global Positioning System constraints on the active tectonics of NE Iran and the South Caspian region, *Earth Planet. Sci. Lett.*, 2013, vols. 377–378, pp. 287–298. https://doi.org/10.1016/j.epsl.2013.07.007

Mouthereau, F., Lacombe, O., and Vergés, J., Building the Zagros collisional orogen: Timing, strain distribution and the dynamics of Arabia/Eurasia plate convergence, *Tectonophysics*, 2012, vols. 532–535, pp. 27–60. https://doi.org/10.1016/j.tecto.2012.01.022

Nilforoushan, F., Masson, F., Vernant, P., Vigny, C., Martinod, J., Abbassi, M., Nankali, H., Hatzfeld, D., Bayer, R., Tavakoli, F., Ashtiani, A., Doerflinger, E., Daignières, M., Collard, P., and Chéry, J., GPS network monitors the Arabia-Eurasia collision deformation in Iran, *J. Geod.*, 2003, vol. 77, nos. 7–8, pp. 411–422. https://doi.org/10.1007/s00190-003-0326-5

Nissen, E., Yamini-Fard, F., Tatar, M., Gholamzadeh, A., Bergman, E., Elliott, J.R., Jackson, J.A., and Parsons, B., The vertical separation of mainshock rupture and microseismicity at Qeshm island in the Zagros fold-and-thrust belt, Iran, *Earth Planet. Sci. Lett.*, 2010, vol. 296, nos. 3–4, pp. 181–194. https://doi.org/10.1016/j.epsl.2010.04.049

Peyret, M., Djamour, Y., Hessami, K., Regard, V., Bellier, O., Vernant, P., Daignières, M., Nankali, H., Van Gorp, S., Goudarzi, M., Chéry, J., Bayer, R., and Rigoulay, M., Present-day strain distribution across the Minab-Zendan-Palami fault system from dense GPS transects, *Geophys. J. Int.*, 2009, vol. 179, no. 2, pp. 751–762. https://doi.org/10.1111/j.1365-246X.2009.04321.x

Raeesi, M., Zarifi, Z., Nilfouroushan, F., Boroujeni, S.A., and Tiampo, K., Quantitative analysis of seismicity in Iran, *Pure Appl. Geophys.*, 2017, vol. 174, no. 3, pp. 793–833. https://doi.org/10.1007/s00024-016-1435-4

Regard, V., Bellier, O., Thomas, J.-C., Abbassi, M.R., Mercier, J.L., Shabanian, E., Feghhi, Kh., and Soleymani, S., Accommodation of the Arabia-Eurasia convergence in the Zagros-Makran transfer zone, SE Iran: A transition between collision and subduction through a young deforming system, *Tectonics*, 2004, vol. 23, no. 4, p. TC4007. https://doi.org/10.1029/2003TC001599

Regard, V., Bellier, O., Thomas, J.C., Bourlès, D.L., Bonnet, S., Abbassi, M., Braucher, R., Mercier, J.L., Shabanian, E., Soleymani, Sh., and Feghhi, Kh., Cumulative right-lateral fault slip rate across the Zagros–Makran transfer zone: role of the Minab–Zendan fault system in accommodating Arabia–Eurasia convergence in southeast Iran, *Geophys. J. Int.*, 2005, vol. 162, no. 1, pp. 177–203. https://doi.org/10.1111/j.1365-246X.2005.02558.x

Reilinger, R., McClusky, S., Vernant, Ph., Lawrence, S., Ergintav, S., Cakmak, R., Ozener, H., Kadirov, F.,

Guliev, I., Stepanyan, R., Nadariya, M., Hahubia, G., Mahmoud, S., Sakr, K., ArRajehi, A., Paradissis, D., Al-Aydrus, A., Prilepin, M., Guseva, T., Evren, E., Dmitrotsa, A., Filikov, S.V., Gomez, F., Al-Ghazzi, R., and Karam, G., GPS constraints on continental deformation in the Africa-Arabia-Eurasia continental collision zone and implications for the dynamics of plate interactions, *J. Geophys. Res.*, 2006, vol. 111, no. B5, p. B05411.
https://doi.org/10.1029/2005JB004051

Ritz, J.-F., Nazari, H., Ghassemi, A., Salamati, R., Shafei, A., Solaymani, S., and Vernant, Ph., Active transtension inside central Alborz: A new insight into northern Iran–southern Caspian geodynamics, *Geology*, 2006, vol. 34, no. 6, pp. 477–480.
https://doi.org/10.1130/G22319.1

Shahvar, M.P. and Zaré, M., The 27 august 2010 Mw 5.7 Kuh-Zar earthquake (Iran): Field investigation and strong-motion evidence, *Nat. Hazards*, 2013, vol. 66, no. 2, pp. 689–706.
https://doi.org/10.1007/s11069-012-0507-8

Sudhaus, H. and Jonsson, S., Source model for the 1997 Zirkuh earthquake (M_w = 7.2) in Iran derived from JERS and ERS InSAR observations, *Geophys. J. Int.*, 2011, vol. 185, no. 2, pp. 676–692.
https://doi.org/10.1111/j.1365-246X.2011.04973.x

Talebian, M. and Jackson, J.A., Offset on the main recent fault of the NW Iran and implications for the late Cenozoic tectonics of the Arabia–Eurasia collision zone, *Geophys. J. Int.*, 2002, vol. 150, no. 2, pp. 422–439.
https://doi.org/10.1046/j.1365-246X.2002.01711.x

Talebian, M. and Jackson, J.A., A reappraisal of earthquake focal mechanisms and active shortening in the Zagros mountains of Iran, *Geophys. J. Int.*, 2004, vol. 156, no. 3, pp. 506–526.
https://doi.org/10.1111/j.1365-246X.2004.02092.x

Tatar, M., Hatzfeld, D., Martinod, J., Walperdorf, A., Ghafori-Ashtiany, M., and Chéry, J., The present-day deformation of the central Zagros from GPS measurements, *Geophys. Res. Lett.*, 2002, vol. 29, no. 19, pp. 33-1–33-4.
https://doi.org/10.1029/2002GL015427

Tavakoli, F., Walpersdorf, A., Authemayou, C., Nankali, H.R., Hatzfeld, D., Tatar, M., Djamour, Y., Nilforoushan, F., and Cotte, N., Distribution of the right-lateral strike–slip motion from the Main Recent Fault to the Kazerun Fault System (Zagros, Iran): Evidence from present-day GPS velocities, *Earth Planet. Sci. Lett.*, 2008, vol. 275, nos. 3–4, pp. 342–347.
https://doi.org/10.1016/j.epsl.2008.08.030

Vernant, Ph., Nilforoushan, F., Hatzfeld, D., Abbassi, M.R., Vigny, C., Masson, F., Nankali, H., Martinod, J., Ashtiani, A., Bayer, R., Tavakoli, F., Chéry, J., Present-day crustal deformation and plate kinematics in Middle East constrained by GPS measurements in Iran and northern Oman, *Geophys. J. Int.*, 2004a, vol. 157, no. 1, pp. 381–398.
https://doi.org/10.1111/j.1365-246X.2004.02222.x

Vernant, Ph., Nilforoushan, F., Chéry, J., Bayer, R., Djamour, Y., Masson, F., Nankali, H., Ritz, J.-F., Sedighi, M., and Tavakoli, F., Deciphering oblique shortening of central Alborz in Iran using geodetic data, *Earth Planet. Sci. Lett.*, 2004b, vol. 223, nos. 1–2, pp. 177–185.
https://doi.org/10.1016/j.epsl.2004.04.017

Walker, R.T. and Jackson, J., Active tectonics and late Cenozoic strain distribution in central and eastern Iran, *Tectonics*, 2004, vol. 23, no. 5, p. TC5010.
https://doi.org/10.1029/2003TC001529

Walker, R.T., Gans, P., Allen, M.B., Jackson, J., Khatib, M., Marsh, N., and Zarrinkoub, M., Late Cenozoic volcanism and rates of active faulting in eastern Iran, *Geophys. J. Int.*, 2009, vol. 177, no. 2, pp. 783–805.
https://doi.org/10.1111/j.1365-246X.2008.04024.x

Walpersdorf, A., Hatzfeld, D., Nankali, H., Tavakoli, F., Nilforoushan, F., Tatar, M., Vernant, P., Chéry, J., and Masson, F., Difference in the GPS deformation pattern of North and Central Zagros (Iran), *Geophys. J. Int.*, 2006, vol. 167, no. 3, pp. 1077–1088.
https://doi.org/10.1111/j.1365-246X.2006.03147.x

Walpersdorf, A., Manighetti, I., Mousavi, Z., Tavakoli, F., Vergnolle, M., Jadidi, A., Hatzfeld, D., Aghamohammadi, A., Bigot, A., Djamour, Y., Nankali, H., and Sedighi, M., Present-day kinematics and fault slip rates in eastern Iran, derived from 11 years of GPS data, *J. Geophys. Res.*, 2014, vol. 119, no. 2, pp. 1359–1383.
https://doi.org/10.1002/2013JB010620

Yunga, S.L., *Metody i rezul'taty izucheniya seismotektonicheskikh deformatsii* (Methods and Results of Studying Seismotectonic Deformations), Moscow: Nauka, 1990.

Zarifi, Z., Nilfouroushan, F., and Raeesi, M., Crustal stress map of Iran: Insight from seismic and geodetic computations, *Pure Appl. Geophys.*, 2014, vol. 171, no. 7, pp. 1219–1236.
https://doi.org/10.1007/s00024-013-0711-9

Translated by A. Carpenter